Università degli Studi di Padova

Dipartimento di Fisica & Astronomia "G. Galilei"

Corso di Laurea Magistrale in Fisica

Tesi di Laurea Magistrale

Electrochemical growth of silicon nanostructures for photovoltaic applications

---

Relatore: Prof. Giovanni Mattei
Correlatore: Dr. Esther Alarcón Lladó

Controrelatore: Prof. Enrico Napolitani

Laureando: Laura Canil
Matricola: 1109018

A.A. 2016-2017

Contents

Abstract

Silicon is the most widely used material for current photovoltaic (PV) panel manufacturing. Next generation solar cells will be obtained by creating novel device structures, material fabrication processes and implementing new physical principles. In this regard, semiconductor nanostructures have shown their potential for achieving efficient solar energy conversion at low cost due to their particular and tunable optical properties.

Nevertheless, most of the fabrication techniques currently employed have some limiting factors, such as the need for high temperatures (T > 500 °C) or vacuum systems. For this reason in this work the growth of Si nanostructures has been investigated through the combination of a cost-effective technique like electrochemical deposition with the properties of liquid Ga as catalyst for the crystallization.

Electrodeposition has been performed successfully on different substrates and for different temperatures and voltages. The results have been analyzed through SEM, EDX and XPS revealing a correlation between temperature/voltage and the oxidation state and homogeneity of the deposition. The actual effect of Ga in the process is not clear, but it seems that under the current conditions Ga is not really playing a role. Further experiments are planned to better understand the system and hopefully obtaining crystalline Si nanostructures exploiting the role of Ga as catalyst.

Sommario

Il silicio è di gran lunga il materiale più utilizzato per la produzione di pannelli fotovoltaici. La prossima generazione di celle solari sarà basata sullo sviluppo di nuovi processi di fabbricazione e sullo sfruttamento di nuovi principi fisici. A questo proposito nanostrutture di materiali semiconduttivi, grazie alle loro particolari e regolabili proprietà ottiche, si sono dimostrate promettenti allo scopo di migliorare l'efficienza nella conversione dell'energia solare.

Lo svantaggio è che la maggiorparte delle tecniche di fabbricazione attualmente utilizzate sono limitate dalla necessità di condizioni particolari, come temperature molto alte (T > 500

°C) o l'utilizzo di sistemi di vuoto. Per questo motivo in questo lavoro di tesi si è indagato un nuovo metodo per la fabbricazione di nanostrutture di silicio, basato sulla combinazione di una tecnica relativamente semplice e economicamente vantaggiosa come l'elettrodeposizione e lo sfruttamento delle proprietà del Ga liquido come catalizzatore per la cristallizzazione. Silicio è stato elettrodepositato con successo su diversi substrati e per diverse temperature e voltaggi. I risultati sono stati analizzati attraverso SEM, EDX e XPS, mostrando una correlazione tra temperatura/voltaggio e lo stato di ossidazione e omogeneità della deposizione. Il ruolo del gallio nel processo non è tuttavia chiaro, alle attuali condizioni non sembra avere un vero effetto sulla deposizione. Ulteriori esperimenti sono previsti allo scopo di comprendere meglio il comportamento del sistema e auspicabilmente ottenere nanostrutture di silicio cristallino sfruttando il ruolo del Ga come catalizzatore.

Introduction

One of the greatest challenges facing mankind is to make clean energies become the primary resource to fuel our economies. Solar cells are one of the most promising and important contributions for this purpose and today crystalline silicon (c-Si), thanks to its Earth-abundance and suitable electronic properties (its 1.1 eV bandgap is optimal for capturing the solar spectrum using a single-junction device), is the most important semiconductor material for photovoltaic (PV) industries.

Nevertheless, the optical properties of c-Si are relatively poor, because of its indirect bandgap which precludes an efficient emission and absorption of light. This is a considerable weakness and high performance in all aspects of optical functionality is highly desired, as it would enable true optoelectronic integration and pave the way to faster, highly integrated and low-cost devices.

Currently the highest demonstrated photovoltaic conversion efficiency of a Si solar cell is near 25%, which has been realized in a single junction configuration [1]. This is very close to the Shockley-Queisser limit of about 30% [2], and therefore only limited further progress can be expected. Wafer-based "bulk" silicon cells currently dominate the market, but higher optoelectronic performance would be the enabler of a new generation of high-efficiency Si solar cells. This introduces the need for light-trapping schemes that at the same time increase the effective absorption length and reduce the path-length for carrier extraction. Using solar cells with nanostructured radial p-n junctions may be a good solution and boost the efficiency of photovoltaic energy conversion, overcoming some of the restraints that lead to the Shockley-Queisser limit [3].

For these reasons nanostructures (NS) and their particular and tunable optical properties[4][5] are becoming of great interest in the photovoltaic field and the aim of this work is to explore a new cost-effective and non-energy intensive technique to grow Si nanostructures.

One of the main challenges related to the implementation of NS in the development of solar cells is the fabrication process. Current industrial manufacturing methods for semiconductors are energy- and resource-intensive, these approaches are in general multi-step processes and often involve limiting factors such as the need for high temperatures (T > 500 °C) or vacuum systems [6]. This is the reason why in this work it is investigated the employment of a comparatively non-energy-intensive technique for the growth of Si nanostructures: electrochemical deposition.

Electrodeposition has long been explored as a possible alternative route for Si preparation. The principal advantages are the comparatively simple instrumentation/setup and the possibility of deposition at low temperatures (T < 500 °C). "Conventional" electrodeposition is defined by solid electrodes immersed in an electrolyte bath with dissolved oxidized precursors, a negative potential applied to the solid cathode drives the electroreduction of the precursor's ions to the zero-valent state and consequently their deposition on the surface of the cathode.
The main challenge related to the electrochemical growth of NS at low temperature is that the product is always a highly impure amorphous solid, which means that additional thermal annealing and purification are required for an electrodeposition process to yield crystalline Si [7][8], indeed until now this has severely limited the appeal of Si electrodeposition. Nevertheless, recently has been reported a new electrodeposition method which allows to obtain crystalline semiconductors at low temperatures, this technique is called *electrochemical liquid-liquid-solid process* (ec-LLS)[9]. The concept is using a liquid-metal electrode which acts either as cathode, so as source of electrons for the reduction process, and as solvent for recrystallization. Through this tactic it has been already possible to achieve direct electrodeposition (i.e. reduction of dissolved precursor to give fully reduced crystalline material without need for subsequent annealing) of single-crystalline Ge nanowires [10], and GaAs [11] and Si [12] crystalline films.
In particular crystalline Si has been obtained through electroreduction of $SiCl_4$ in propylene carbonate at 80°C, using a liquid Ga pool as working electrode. This result represents the main inspiration for the present work, the prospect is electrodepositing Si through a liquid-liquid-solid process, but using liquid Ga seeds instead of a liquid Ga pool, so that the seeds may act both as catalysts for the crystallization and as template for the shape of the growing nanostructures.
In the present work therefore is performed Si electrodeposition combined with the employment of liquid Ga seeds as catalysts for crystallization, according to the ec-LLS process. The final goal is obtaining Si crystalline nanostructures through a cost-effective one-step process at low temperature, but the main purpose of this work is analyzing how different parameters, such as temperature, applied voltage and substrate, can affect the deposition, with the prospect of finding the best conditions for the growth of Si NS. Electrochemical tests are hence carried out at various conditions and the grown material is analyzed and characterized with various techniques, such as SEM, EDX and XPS.

The present thesis is organized as follows:
Chapter 1 Quick review about the importance of nanostructures in photovoltaics and some of the currently most used fabrication techiques.
Chapter 2 Introduction to the basic principles of electrochemistry and theoretical description of the electrodeposition process.
Chapter 3 Electrodeposition and LLS-process applied to silicon.

Chapter 4 Description of the fabrication process.

Chapter 5 Description of the techniques employed for the characterization.

Chapter 6 Experimental results and effect of different parameters on the deposition.

CHAPTER 1

Si nanostructures for photovoltaics

Silicon is the prime candidate for realizing large-scale photovoltaic systems. It has been demonstrated that, thanks to their good optoelectronic properties, silicon nanostructures can enhance the performance of solar cells [13][3], moreover, because of the quantum confinement, the energy structure in a nanoconfiguration is influenced directly by its size and therefore can accordingly be tuned almost at will [14].
Si nanocrystals and especially Si nanowires present several properties of importance for photovoltaics. Silicon nanowires solar cells have already been fabricated both on a single wire [24] and on nanowires arrays [25]. Two main schemes are used: axial junctions [26], in which the p-i-n diode is fabricated along the length of the nanowire by varying the doping density during growth, and radial junctions [27], in which the diode is fabricated coaxially by a core-shell method.
There are many advantages in using silicon nanowires for solar cells: first of all, since the light remains trapped inside the nanowires forest by multiple scattering events, nanowire arrays are extremely strong absorbers. Second, radial junctions have the advantage of a very short electrical path-length for carrier extraction and this has the potential for significant performance improvements. Therefore the resulting solar cells have all the advantages of a highly absorbing material with a radial, low-path, carrier extraction.

1.1 Fabrication techniques

Because of the interesting properties of Si nanostructures for photovoltaics, many techniques have been developed for their fabrication. In this section the most important techniques currently employed for growing Si nanostructures are briefly presented [6].

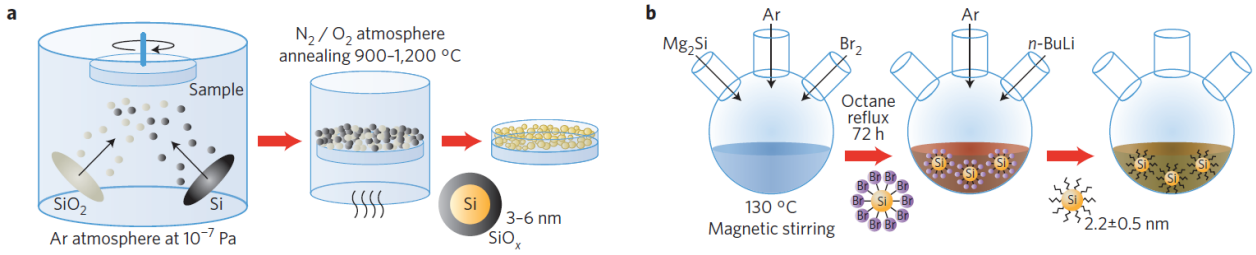

Figure 1.1: Nanocrystals fabrication techniques [6]: (a) self assembly, (b) colloidal chemistry.

The most successful methods for fabricating Si nanocrystals are *self-assembly* from Si-rich silicon oxide matrices and *colloidal chemistry* (fig. 1.1).

Self-assembly

A film of SiO_x (with $x < 2$) is formed by a thin-film deposition technique, such as magnetron sputtering or chemical vapour deposition (CVD), or by implantation of a SiO_2 layer with a high dose of silicon ions. Subsequently the film is annealed at high-temperature (typically above 800 °C) and this produces a phase separation between Si and SiO_2 with the formation of Si nanoclusters that grow by Ostwald ripening [28]. The dimensions, crystallinity and size distribution of the nanoclusters depend on the Si excess, the temperature and the annealing time. A variation of this method is to form a periodic structure of alternating layers of SiO_x and SiO_2 (superlattice) [29]. In this case it is possible to control the precipitation of Si nanoclusters in the SiO_x layers by controlling the thickness of the layers, the result is a much narrower size distribution.

Colloidal chemistry

Different kind of colloidal solutions can be employed for obtaining Si nanocrystals. These solutions can be made from freestanding porous Si [30], plasma-synthesized powders [31], or synthesized directly using the sol-gel method or a variety of wet-chemical processes [32].
Especially interesting properties have been reported for colloidal Si nanocrystals prepared by a wet-chemical oxidation–reduction method [33]. In the case of the reported paper Mg_2Si is prepared by reacting Mg in a 1% excess with Si powder at 700 °C for 3 days in a sealed tube, then Si nanostructures are prepared by the reaction of $SiCl_4$ with Mg_2Si in ethylene glycol dimethyl ether (glyme) and surface-terminated with various alkyl groups, finally this mixture has to be refluxed for 36 or 48h, under dry, deoxygenated argon. This kind of synthesis yields photostable and freestanding n-butyl-terminated Si nanocrystals of typically 2-3 nm in diameter.

There are also several methods for preparing Si nanowires, the most commonly used are *chemical etching* [34], *nanolithography* [35] and *vapour-liquid-solid process* (VLS) [36].

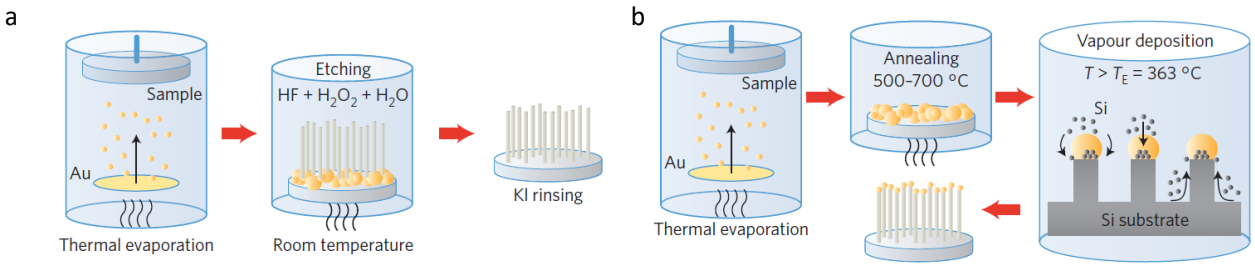

Figure 1.2: Nanowires fabrication techniques [6]: (a) metal-assisted chemical etching (MACE), (b) vapour-liquid-solid process (VLS).

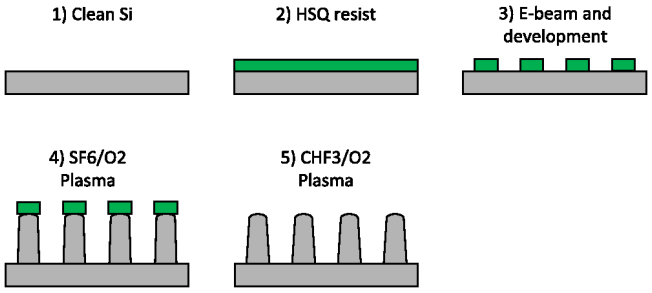

Figure 1.3: Example of nanopillars obtained through a nanolithography process [35].

Chemical etching

In this method an array of Si nanowires is formed by chemical etching of a Si wafer at room temperature. A metal salt is usually used to catalyze silicon etching within an aqueous H_2O_2/HF solution, this typically forms metallic structures on top of the nanowires, which can be removed, but results in damage to the nanowires.
A better method (which doesn't produce damages on the nanowires) is to etch using an ultrathin metallic film in place of the metal salts. The metal acts as a catalyst for the etching process, indeed the oxidant is preferred to be reduced at the surface of the metal and therefore the process occurs preferentially underneath the metal, if the metal film is patterned in a way in which small regions are uncovered, these regions represent the sites for the nanowires formation. The size of the nanowires can be therefore controlled by changing the metallic pattern or by coupling the metal deposition with lithography or nanosphere self-assembly. The major drawback is the multi-step process for the formation of the Si to be etched, since it involves electron beam evaporation and crystallization processes at high (> 500°C) temperatures [34].

Nanolithography

Nanolithography is a powerful top-down technique which allows to obtain very regular nanopillars array. Nanopillars are formed with a mask and a highly anisotropic reactive ion etching (RIE) process. The mask is generally created by electron beam lithography, in which custom shapes are "drawn" by a focused beam of electrons on a surface covered with an electron-sensitive film or resist. Then the sample undergoes a RIE process, in which high-energy ions (generated under low pressure) from a chemically reactive plasma hit the sample surface and react with it, etching chemically the material. Other etching processes, for example with a different kind of plasma, can be applied to remove resist residuals or to make the nanopillars more thin [37].

Vapour-liquid-solid method (VLS)

VLS process is probably the most employed method for the fabrication of nanowires [36]. In this technique a liquid metal is used as catalyst for the growth, for silicon this metal is often Au. The metal droplets are formed on a silicon surface by lithography or self-assembly, heated to temperatures above the Au-Si eutectic point (T$\sim$ 360°C) and exposed to a Si precursor in gaseous phase. The precursor is decomposed to its zero-valent form and enter the droplets: when saturation is reached Si precipitates growing nanowires below the droplets with the droplets being pushed up. The whole process is happening under vacuum. A very similar technique is the *solution-liquid-solid process* (SLS), in this case Si is not in gas-phase, but dissolved in a hot liquid solvent free of any water or O_2 [38].
VLS and SLS have proven useful for the synthesis and study of micro and nanocrystalline materials, but also present some drawbacks as fabrication strategies. High temperatures and/or low pressures are required to drive the thermal decomposition of the precursors to their zero-valent forms. Moreover both techniques employ heavily refined and expensive semiconductor precursor compounds that are often toxic and are themselves resource-intensive to synthesize, handle, and store. And finally, the combination of high temperature, low pressure, and harmful precursors imposes serious constraints on the choice of deposition substrates and metal catalyst.

The techniques described in this chapter are nowadays commonly used, but all of them have in common the need for either high temperatures, vacuum systems or highly refined chemicals, and often are processes which include multiple steps. For this reason in this work it has been chosen to employ, instead, electrochemical deposition, which needs a comparatively simple instrumentation/setup and the possibility of deposition at low temperatures.

CHAPTER 2

Electrochemistry

Electrochemistry is the branch of physical chemistry that examines the phenomena resulting from combined chemical and electrical effects. It can be divided into the study of chemical changes caused by the passage of an electric current and the production of electrical energy by chemical reactions. The field includes a lot of different phenomena, like electrophoresis or corrosion, and is at the basis of devices like batteries and fuel cells or technologies such as the electroplating of metals.

2.1 Principles

Electrochemical systems are related to the transport of charge across the interface between chemical phases. In general there's an electronic conductor, called *electrode*, in which the charge is transported by the movement of electrons, and an ionic conductor, the *electrolyte*, in which the charge is carried by the movement of ions. The most simple system consists of two electrodes separated by one electrolyte phase, but connected by an external circuit. This system is named *electrochemical cell*.
The reactions which take place at the electrode-electrolyte interface and involve charge exchange are called half-cell reactions and can be divided into *reduction* and *oxidation* reactions, a reaction is classified as oxidation or reduction depending on the direction of electron transfer. The overall chemical reaction of the cell is given by combining the two individual half cell reactions and is called *redox reaction*, by convention the electrodes at which the oxidation and reduction reactions occur are named respectively *anode* and *cathode*.
Reduction involves the transfer of electrons (e) from the electrode to the species A in the electrolyte:

$$A + e^- \rightarrow A^- \tag{2.1}$$

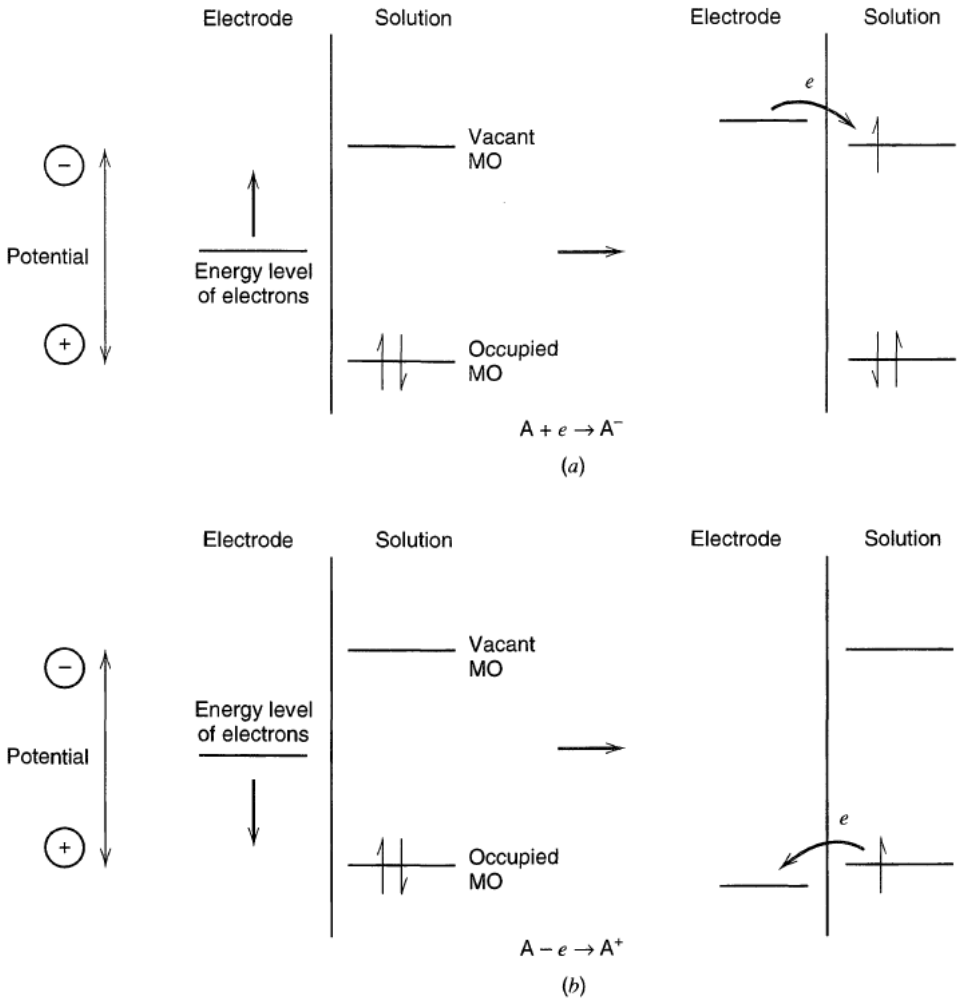

Figure 2.1: Representation of (a) reduction and (b) oxidation process of species A in solution. The shown molecular orbitals (MO) of species A are the highest occupied MO and the lowest vacant MO [39].

It is an energetic process, in the beginning the energy level of the electrons in the electrode is lower than the electronic state of the species in the electrolyte, but by driving the electrode to more negative potentials, for example through a battery or a power supply, the energy of the electrons is raised and it becomes more favorable for the system to transfer the electrons into vacant electronic states on species in the electrolyte (fig. 2.1a).
Oxidation instead involves the transfer of electrons from the species to the electrode:

$$A - e \rightarrow A^{+} \tag{2.2}$$

This is again an energetic process and occurs when the energy of the electrode is lowered below the highest occupied molecular orbital of the compound (fig. 2.1b).
Every reaction has a particular potential, called *standard potential (E_0)*, which needs to be reached so that these processes can occur and it depends on the chemical substances in the system. Tabulations for E_0 of most half-cell reactions are available in literature or on-line

and are in general referred to the standard hydrogen electrode (SHE). The E_0 of SHE is the potential of H reduction:

$$2H^+_{(aq)} + 2e^- \rightarrow H_{2(g)} \tag{2.3}$$

which is declared to be 0V at all temperatures [1] [40].
The cell potential is then calculated as the sum of the reduction potential for the cathode and the oxidation potential for the anode. To calculate the reduction potential of an electrochemical reaction (half-reaction or full-reaction) in relation to SHE, temperature, and activities (often approximated by concentrations) of the chemical species undergoing reduction and oxidation is generally employed the Nernst equation:

$$E = E_0 + \frac{RT}{nF} ln \frac{C_O}{C_R} \tag{2.4}$$

where E_0 is the standard reduction potential of the species, R is the gas constant, T the temperature, n the number of electrons transferred in the half-reaction, F the Faraday constant and C_O and C_R the concentrations of the oxidized\reduced species. The standard potential undergoes therefore a shift related to the concentration.

2.2 Electrochemical cells

As mentioned in the previous section, an electrochemical cell is a system which combines electronic and ionic conductors in order to generate electricity from a spontaneous redox reaction (*galvanic cell*) or that uses electricity to drive a non spontaneous redox reaction (*electrolytic cell*), which is the case of this work. A standard electrochemical cell includes three electrodes called *working electrode* (WE), *reference electrode* (RE) and *counter electrode* (CE), the setup is shown in fig. 2.2 and will be described later.

Working electrode: is the electrode in which the reaction of interest is occurring. Standard WEs include [41] the noble metals (especially gold and platinum), carbon (including pyrolytic carbon, glassy carbon, carbon paste, nanotubes and vapordeposited diamond), liquid metals (mercury and its amalgams) and semiconductors (indium-tin oxide, Si), but in the end any conducting element can be exploited.

Reference electrode: is an electrode which has a stable and well-known potential which doesn't change with the passage of current (*ideal nonpolarizable electrode*), it is used as a point of reference in the electrochemical cell for the potential control and measurement. The high

[1] The estimated absolute electrode potential of the hydrogen electrode is 4.44 ± 0.02 V at 298.15 K [40].

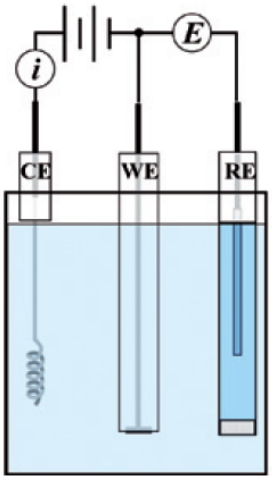

Figure 2.2: Schematic representation of three-electrode electrochemical cell [41].

stability of the reference electrode potential is usually reached by employing a redox system with constant concentrations of each participants of the redox reaction, moreover the current flow through the reference electrode is kept close to zero (ideally, zero). A noble metal electrode (i.e. a platinum wire) may be employed as reference electrode and is than called *quasi-reference electrode* (QRE). In this case the potential is still stable but not well defined as in a common RE, nevertheless it can be advantageous because of its simplicity and because there is no risk of contamination of the solution by solvent molecules or ions that a conventional reference electrode might transfer.

Counter electrode: it is also known as *auxiliary electrode*, it is an electrode which is used to close the current circuit in the electrochemical cell, it is usually made of an inert material (i.e. Pt, Au, graphite, glassy carbon). Because the current is flowing between the WE and the CE, the total surface area of the CE (source/sink of electrons) should be higher than the area of the WE so that it will not be a limiting factor in the kinetics of the electrochemical process under investigation.

When a potential is applied to the cell, the ions in the solution are attracted towards the electrode with the opposite charge and as soon as E_0 is reached a redox reaction occurs.

2.2.1 Three-electrode cell

Three-electrode cells (fig. 2.2) are the commonly used setup in electrochemical studies. In this case, the current flows between the CE and the WE, but the potential difference is measured

between the RE (kept at close proximity of the WE) and the WE. Since no (or little) current passes to the RE, it is a reliable reference for potential control. The potential between the WE and CE usually is not measured, but the voltage applied to the CE is adjusted so that the potential difference between the WE and RE will be equal to the potential difference specified by the user. Moreover the current measured at the WE is not limited by reactions occurring at the CE, but is just determined by the reactions at the WE.
Since the potential applied to the cell is the potential of the WE with respect to the RE, this is equivalent to observing or controlling the energy of the electrons within the working electrode. By driving the electrode to more negative\positive potentials the energy of the electrons is than raised\lowered until a reduction\oxidation current starts flowing.

Potentiostat

A three-electrode cell is run through an electronic hardware called *potentiostat*, which controls the potential difference between WE and a RE by changing the voltage applied to the CE in the manner shown in fig. 2.3.

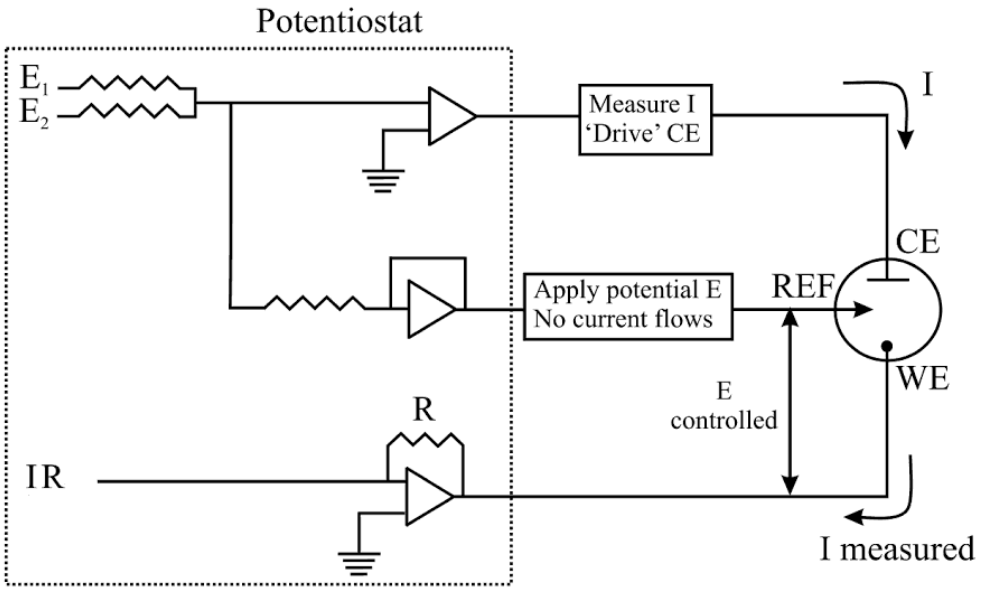

Figure 2.3: Scheme of the circuit of a potentiostat. E_1 and E_2 represent the input signal, E is the desired potential for the working electrode, R is a variable resistance while all the others are equal, I is the current flowing [42].

The device imposes a fixed potential $E = (\Phi_M - \Phi_S)_{working} - (\Phi_M - \Phi_S)_{reference}$, where Φ_M and Φ_S are the electrical potentials of the metal electrode and the solution. Since the value of $(\Phi_M - \Phi_S)_{reference}$ is constant, any changes in E are reflected as changes in $(\Phi_M - \Phi_S)_{working}$. The imposition of the potential drop $(\Phi_M - \Phi_S)_{working}$ on the WE\solution interface will cause

a current to flow, that is what is studied (as a function of the controlled applied potential) during an experiment. The role of the CE is to pass the same current as that induced to flow through the WE, for this purpose the potentiostat drives the CE to the voltage required to pass this current.
It's important to underline that it is possible to apply a controlled potential at the working electrode only because of the presence of three electrodes, and this is one of the reason why this configuration is the most commonly electrochemical setup used (often preferred to a two-electrode configuration) and is also the one employed in the experiment described in this work.

Techniques

With a three-electrode cell configuration, and thanks to a software which controls the potentiostat[2], it is possible to acquire information about electrochemical processes through different techniques. Only the ones employed in this work are explained below.

Cyclic Voltammetry (CV): Cyclic Voltammetry is the most widely used technique to acquire information about electrochemical reactions. The CV technique consists in linearly scanning the potential of the working electrode between two chosen values, E_1 and E_2, during the voltage sweep the potentiostat measures the current resulting from electrochemical reactions occurring at the electrode interface. The cyclic voltammogram is a current response plotted as a function of the applied potential, a typical example is shown in fig. 2.4.
In the case of fig. 2.4, E_1 = 0.5 V, E_2 = -0.5 V and E_0 = 0V. At relatively positive potentials

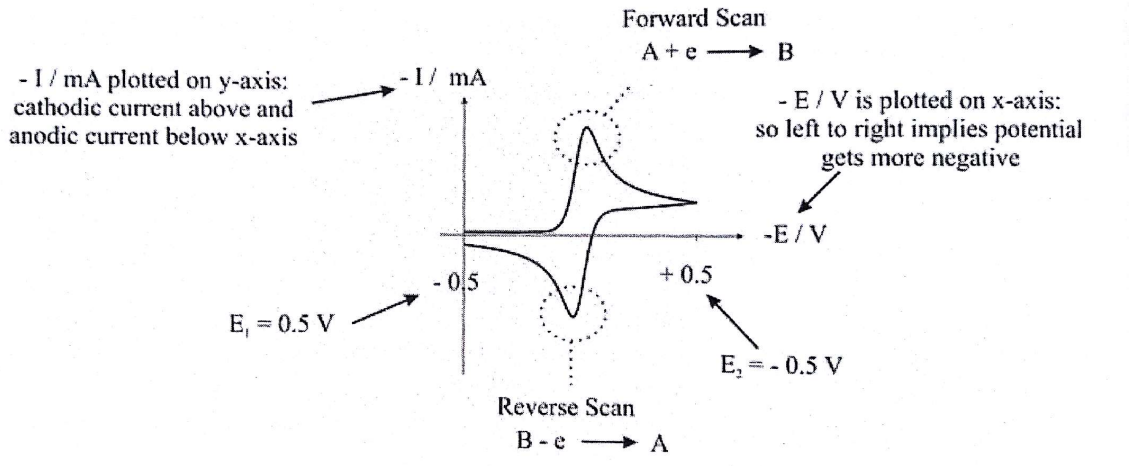

Fig. 4.4

Figure 2.4: Standard voltammogram [42].

[2]In the case of this work the software is EC-Lab

there's no current since the electrode is insufficiently negative to reduce A to B (energetically the situation is the one described in the left part of fig. 2.1). As the potential becomes more negative and reaches E_0 the current starts rising until the point at which the A ions at the electrode/solution interface are completely depleted and therefore the current starts to lower, until it stabilizes because the ions are consumed as fast as mass transfer (diffusion limited current). The reverse scan goes instead from negative to positive potentials, as soon as the current becomes positive (so enters the negative y axes in fig. 2.4) the oxidation reaction starts and the current increases, again until the point at which the reactants (of species B in this case) are consumed and the current starts decreasing until it is limited by diffusion.

Chronoamperometry (CA): in the Chronoamperometry technique a constant potential E is applied for a duration t and the current is measured. This is the method that in this work has been employed for the deposition, once chosen the potential to be applied. A particularly useful feature of this technique is the chance to fix a limit for the deposited charge, which makes more easily comparable experiments performed in different moments.

2.3 Electrodeposition

Electrochemistry is a very wide field, but, since this work aims at the growth of Si nanostructures, the section of main interest is electrodeposition.
Electrochemical deposition of a metal or a semiconductor involves the reduction of its ions from the electrolyte, therefore to perform such an experiment it is necessary to have a solution containing ions of the material to be deposited, a cell with three electrodes and a power supply. This last two have already been described in the previous section.
A typical electrochemical solution is made of a *solvent* and an *electrolyte*. Its main characteristic is to be conductive and this is given by the electrolyte, which consists of two components, the *precursor* and the *supporting electrolyte*. The precursor is the one which defines the deposition, since provides the ions of the element to be deposited. Indeed it includes the chemical species which, once dissolved in a solvent, splits in ions, allowing the redox reaction. The role of the supporting electrolyte is to increase the conductivity of the solution, especially considering that in general the solvent is not conductive.

The process of electrodeposition is related to the reduction of a chemical species, which can be represented by:

$$A^{n+} + ne \rightarrow A \tag{2.5}$$

where A is the species to be deposited and n is the number of electrons (e) needed by an A ion

to reduce. The electrons are provided by an oxidation reaction at the counter electrode, which can be written as:

$$B^{n-} \rightarrow B + ne \tag{2.6}$$

where in this case B is the oxidizing species.
The overall process can be schematized like shown in fig 2.5: once a voltage is applied the negative ions start moving towards the anode (i.e. the counter electrode), where they release the extra electron, at the working electrode the positive ions from the solution capture an electron and deposit on the surface of the WE, where therefore a layer of the desired material starts depositing.

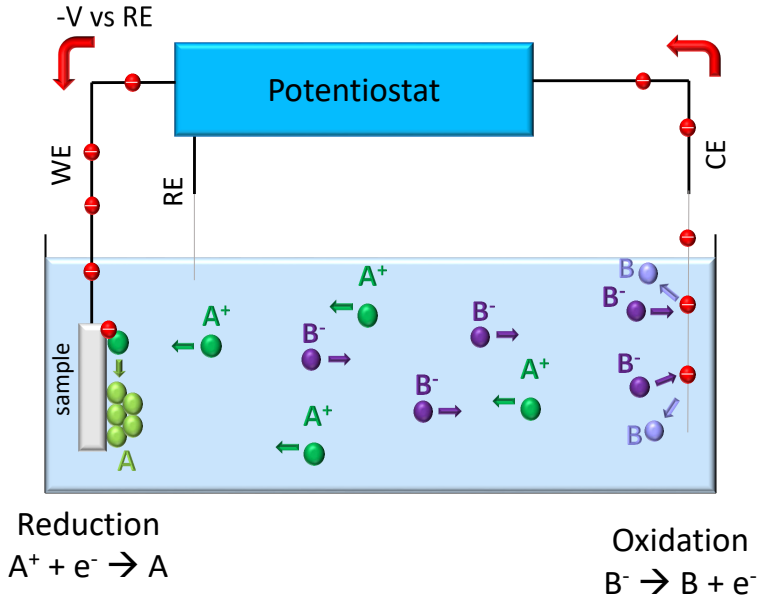

Figure 2.5: Schematic of an electrodeposition process in the most simple case (n = 1)

2.3.1 Electrode-solution interface

The reduction reaction is happening at the working electrode-solution interface, where there is an excess of charge at both the electrode and the solution sides, therefore the behavior is analogous to that of a capacitor. The same is happening at the interface between counter electrode and solution, with opposite charges. knowing this the discussion here will focus only on the WE\solution interface.
At a given potential, there will exist a charge on the metal electrode, q^M, which represents an excess of electrons on the metal surface, and a charge in the solution, q^S, that is made up of an excess of ions in the vicinity of the electrode surface. The charges q^M and q^S are often divided by the electrode area A and expressed as charge densities, such as $\sigma^M = q^M/A$. The

relation between them is always $q^M = -q^S$. The whole array of charges at the interface is called *electrical double layer* and can be schematically represented like in fig. 2.6.

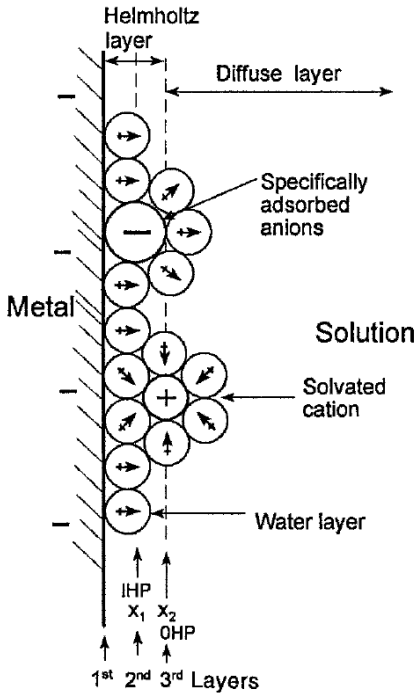

Figure 2.6: Grahame model of the double-layer region under conditions where anions are adsorbed, in this case the polar solvent is water ($\rightarrow$ represents the water dipole and + at the end of the arrow is the positive end of the dipole) [43].

According to the Grahame model [44], the solution side of the double layer is thought to be made up of several "layers". The *inner layer* or *Helmholtz layer*, contains solvent molecules and sometimes other species (ions or molecules) that are said to be specifically adsorbed. The locus of the centers of the specifically adsorbed ions is called *inner Helmoltz plane* (IHP) and is at a distance x_1 from the electrode surface. Solvated ions, instead, are surrounded by a "solvation sphere" and therefore can approach the metal only to a distance x_2. The locus of the centers of the nearest solvated ions (which are said to be nonspecifically adsorbed) is called *outer Helmholtz plane* (OHP). Because of thermal agitation in the solution, the nonspecifically adsorbed ions are distributed in a three-dimensional region called the *diffuse layer*, which extends from the OHP into the bulk of the solution. The thickness of the diffuse layer depends on the total ionic concentration in the solution, for concentrations greater than 10^{-2} M, the thickness is less than $\sim$100 Å.
In this situation the cations are not directly in contact with the electrode surface, but the electrons in the metal can reach the ions through tunnel effect, when the cations capture these electrons they loose the solvation sphere and can deposit on the electrode surface.

2.3.2 Kinetics of electrodeposition

During an electrochemical process the current (or electrode reaction rate) is governed by the rates of processes such as *mass transfer*, *charge transfer* at the electrode surface, *chemical reactions* preceding or following the electron transfer, or other *surface reactions* like adsorption, desorption and electrodeposition itself.
Mass transfer, which is the movement of material in the solution from one location to another, is involved in the overall reaction. It arises either from differences in electrical or chemical potential at the two locations or from movement of a volume element of solution and can be divided in three different modes:

- **Migration**: movement of a charged body under the influence of an electric field (a gradient of electrical potential).
- **Diffusion**: movement of a species under the influence of a gradient of chemical potential (i.e. a concentration gradient).
- **Convection**: stirring or hydrodynamic transport. Generally fluid flow occurs because of natural convection (convection caused by density gradients) and forced convection, and may be characterized by stagnant regions, laminar flow, and turbulent flow.

The rate for each species i is governed by the *Nernst-Planck equation*, written for one-dimensional mass transfer along the x-axis as:

$$J_i(x) = -D_i\frac{\partial C_i(x)}{\partial x} - \frac{z_i F}{RT}D_i C_i\frac{\partial \phi(x)}{\partial x} + C_i v(x) \tag{2.7}$$

where $J_i(x)$ is the flux of species i (mol $s^{-1}cm^{-2}$) at distance x from the surface, D_i is the diffusion coefficient ($cm^2\backslash s$), $\partial C_i\backslash\partial x$ is the concentration gradient at distance x, $\partial\phi(x)\backslash\partial x$ is the potential gradient, z_i and C_i are respectively the valence and concentration (mol cm^{-3}) of the ionic species i, $v(x)$ is the velocity ($cm\backslash s$) with which a volume element in solution moves along the axis, R and F are the gas and Faraday constants and T the absolute temperature. The three terms on the right-hand side represent respectively the contributions of diffusion, migration and convection to the flux.
Mass transport can have important effects on the electrode kinetics, indeed the current can be limited by diffusion and therefore deviate from the Butler-Volmer equation[3], as shown in fig. 2.7. During a reduction reaction the reactant is consumed at the electrode and its concentration at the interface decreases, there is therefore a progressive depletion of the species at the interface

[3]In fig. 2.7 is represented the Butler-Volmer equation for anodic currents, which is $i = i_0 exp\big(\frac{(1-\alpha)zF\eta}{RT}\big)$, where α is the transfer coefficient, η the charge-transfer overpotential, i_0 the exchange current density, F the Faraday constant, R the gas constant and T the temperature

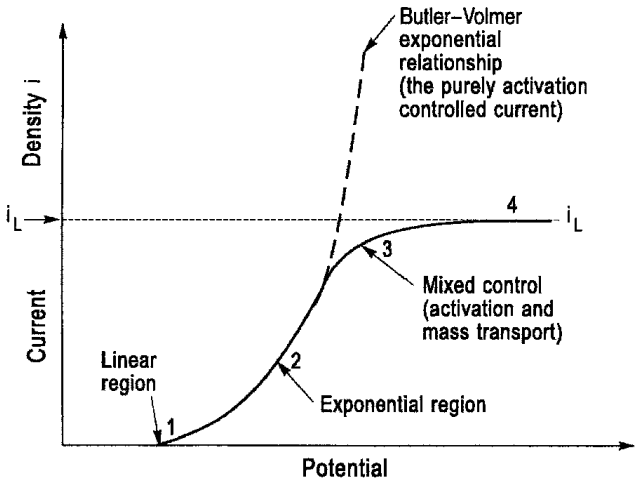

Figure 2.7: The four regions of the current-potential relationship in presence of diffusion limited current i_L [43].

of the electrode and for this reason the reaction can't proceed at a rate faster than the mass transport rate, in this case the current is said to be diffusion limited.

2.4 Liquid-Liquid-Solid crystal growth

As already stressed, electrodeposition has been chosen between other techniques for the growth of nanostructures because it doesn't require any special condition to be performed. Nevertheless it has some drawbacks, for example low-temperature (T < 500 °C) electrodeposition always produces amorphous solids with high impurity content due to the solvent and supporting electrolyte. The poor purity/crystallinity of these films necessitates thermal processing, negating any cost advantage [45] [46]. Moreover high-temperature electrodeposition requires particular solvents, such as the molten salts/fluorides, and the use of sacrificial anodes [47] [7].
This has been a longstanding challenge, but recently direct electrodeposition of crystalline semiconductors has been achieved through a strategy that has been called *electrochemical liquid-liquid-solid process* (ec-LLS) [9] [12].
This strategy marries the semiconductor solvation properties of liquid metal melts with the utility and simplicity of conventional electrodeposition. A low-temperature liquid metal (i.e. Hg or Ga) acts simultaneously as electrode, so as the source of electrons for the reduction of oxidized semiconductor precursors dissolved in an electrolyte, as well as the solvent for dissolution of the zero-valent semiconductor. The liquid electrode can be either a bulk liquid electrode or a nano/microscale liquid metal-droplet electrode, the two cases are shown in fig. 2.8.

In both types, ec-LLS begins with the application of an electrochemical potential to the liquid metal electrode, providing the driving force for reduction of the dissolved precursor to the zero-

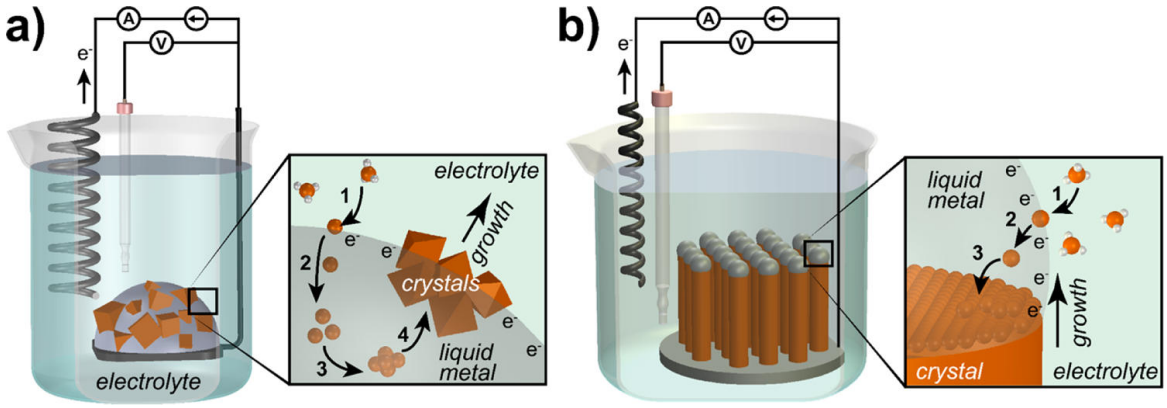

Figure 2.8: Schematic depictions of the experimental setup and steps (insets) of ec-LLS semiconductor crystal growth from (a) bulk and (b) nano/microscale liquid metal-droplet electrodes. ec-LLS proceeds through (1) electrochemical reduction of a dissolved ionic precursor in the electrolyte solution followed by (2) dissolution of the zero-valent semiconductor into the liquid metal electrode. In (a), steps (3) and (4) highlight homogeneous nucleation and subsequent crystal growth, respectively. In (b), step (3) depicts heterogeneous nucleation at a crystal seed interface and subsequent layer-by-layer crystal growth. [9]

valent state (fig. 2.8, step 1). Continued electrochemical reduction of the precursor establishes a concentration gradient between the surface and interior of the liquid metal, which drives dissolution of the semiconductor into the bulk of the liquid metal solution (step 2). When the concentration surpasses the equilibrium solubility of the semiconductor in the metal solution, crystal nucleation (step 3) and growth (step 4) follow. Removal of the electrochemical driving force results in immediate cessation of ec-LLS.

This technique has many advantages, indeed for example, besides allowing the growth of crystalline semiconductor at low temperature, another attractive feature of ec-LLS is the possibility to control the crystal size and shape by modulating the size of the liquid metal electrode [48]. Moreover this technique is not limited by the choice of the substrate, ec-LLS has been performed with liquid metal microdroplets resting on Si wafers, Cu foil, Ti foil, stainless steel, indium tin oxide (ITO) and PEDOT:PPS polymer films, and all substrates supported ec-LLS of Ge nanowires [49]. Electrodeposition of crystalline inorganic semiconductors on organic substrates is particularly attractive from the perspective of device fabrication, representing a unique advantage of ec-LLS.
Different kinds of liquid metals have been investigated, for example Ga-In eutectic (EGaIn) and Ga droplets. It results that all the liquid metals facilitate heterogeneous growth of Ge microwires, but the morphology was particularly sensitive to the electrode composition. For example Ge microwires produced with Ga microdroplets exhibited a smooth (unfaceted) surface and significant taper along the axial direction, after 45 min of growth, the liquid metal cap was completely absent and ec-LLS growth terminated. In contrast, Ge microwires electrodeposited with EGaIn microdroplets were faceted and much less tapered [49]. The specific microscopic

origin of these differences has yet to be identified conclusively, however, since heterogeneous crystal growth models show that the surface tension at a three-phase interface (in this case between the liquid electrolyte, liquid metal and solid semiconductor crystal) strongly influences the crystal growth [50], the ec-LLS observations suggest that changes in surface properties of the liquid metal may be important.

CHAPTER 3

Electrochemical growth of Si nanostructures

In the previous chapter electrodeposition and ec-LLS has been described in a very general way, here instead the focus will be on the application of these techniques to the growth of Si.

3.1 Si electrodeposition

As previously mentioned, a fundamental element for electrodeposition is the solution and it has to contain a solvent, a supporting electrolyte and a precursor. In the case of this work the chosen solvent has been propylene carbonate (PC), the supporting electrolyte tetraethylammonium chloride (TEAC) and the precursor $SiCl_4$, the reasons of this choices and the characteristics of the chemicals involved will be described in section 4.1, here will be instead discussed the electrochemical reaction and the ec-LLS process in the case of Si.

The electrochemical process is summarized in fig. 3.1. The Cl ions are attracted by the CE, where they react to form Cl_2 gas and release electrons, while the Si ions reach the WE and reduce capturing four electrons each. The specific reduction and oxidation reactions are the following:

Reduction reaction: $Si^{4+} + 4e^- \rightarrow Si$
Oxidation reaction: $2Cl^- \rightarrow Cl_2 + 2e^-$

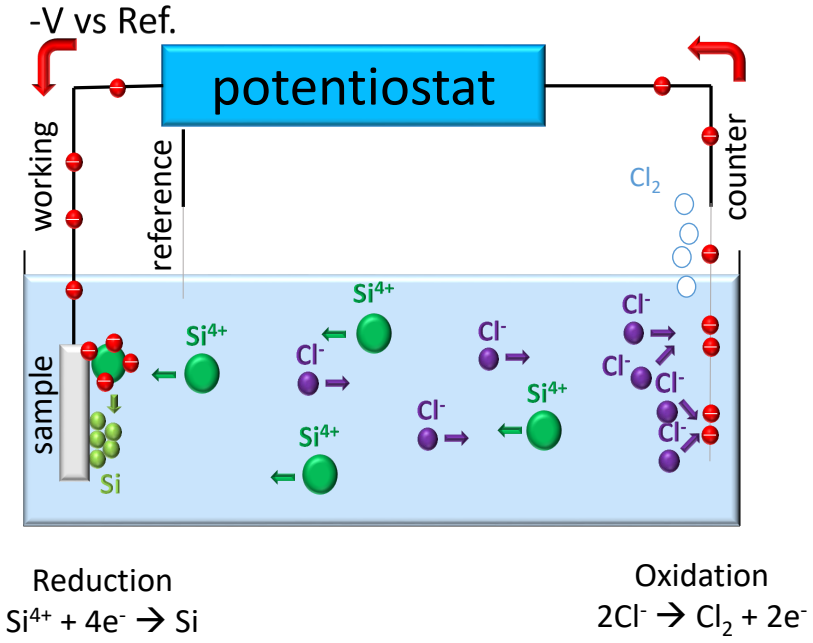

Figure 3.1: Schematic of the electrodepostion process for a solution with $SiCl_4$ as precursor.

3.2 Liquid-liquid-solid process applied to Si

The possibility of growing crystalline Si directly through ec-LLS has been proven by the group of Stephen Maldonado in 2013 [12] and their work provided the basis and idea for this project. They demonstrated the use of a liquid Ga electrode as catalyst for direct electrodeposition of crystalline Si from dissolved precursor under relatively benign conditions. The solution used included propylene carbonate as solvent, 0.2M tetrabutylammonium chloride (TBAC) as supporting electrolyte and 0.5M $SiCl_4$ as precursor.

The process is summarized in fig. 3.2: initially the Si ions (Si^{4+}) are reduced to the zero-valent state (Si) at the electrode-electrolyte interface (step 1), then Si dissolves in the liquid Ga electrode forming a solution of Si and Ga (step 2). If $SiCl_4$ is continually reduced at the electrode-electrolyte interface the solution starts to saturate, when a critical supersaturation condition is reached phase separation of Si(s) from Ga(l) followed by crystal growth occurs (steps 3 and 4).

The deposition has been performed at several temperatures from 80°C up to 200°C and the results have been analyzed with different techniques (SEM, XRD, Raman, EDX and TEM) demonstrating the crystalline nature of the grown material (fig. 3.3).

In the case of this work has been chosen to to exploit this technique for growing crystalline Si, but following a slightly different approach: instead of using a pool of Ga as liquid electrode, the Ga has been deposited on a solid substrate through thermal evaporation (see section 4.3). As

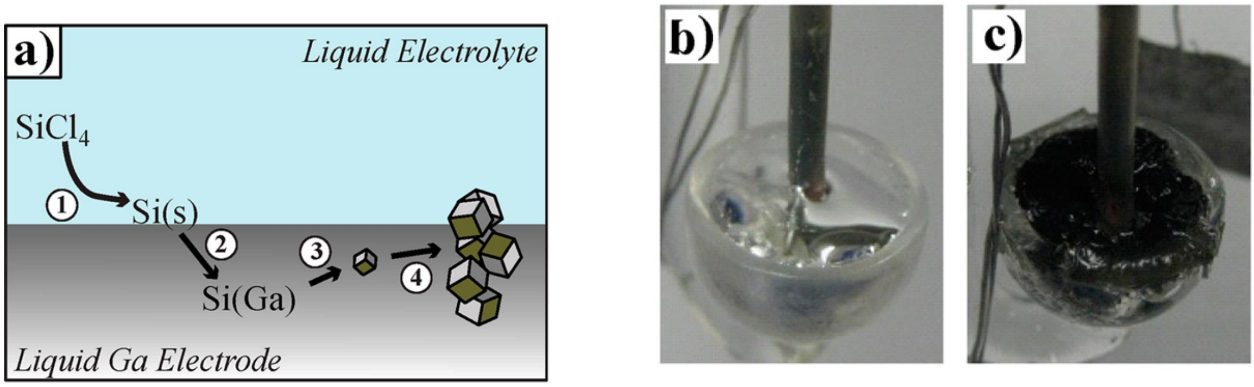

Figure 3.2: (a) Schematic illustration of an electrochemical liquid-liquid-solid process yielding crystalline Si with a liquid Ga [Ga(l)] electrode. (1) Si ions are reduced at the solution/electrode interface. (2) Si dissolves in liquid Ga forming a solution. In (3) and (4) the solution reaches supersaturation and Si precipitates in crystals. (b,c) The Ga pool used as liquid electrode before (b) and after (c) the experiment [12].

will be shown later, using this technique the Ga gathers on the surface forming nanodroplets, which means that the process of crystals formation described for ec-LLS is expected to happen in every single droplet and therefore in this way should be possible to regulate the shape of the nanostructures by tuning the size of the Ga droplets.

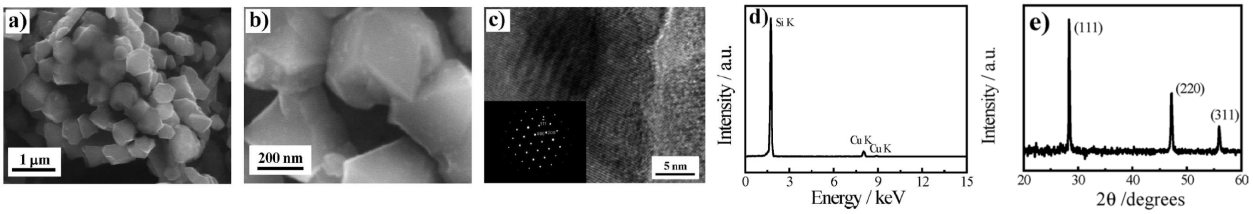

Figure 3.3: (a,b) SEM images of electrodeposited Si at 20000x (a) and 80000x (b) times magnification. (c) High-resolution TEM image of electrodeposited Si at 800000x magnification. Inset: SAED pattern obtained with the electron beam parallel to the [011] zone axis. (d) EDX spectrum of a crystalline Si grain taken in the transmission electron microscope at 300 kV. (e) Xray diffractogram. [12]

3.3 Si-Ga system

As previously underlined, there are different liquid metals with low melting point which can be exploited for ec-LLS process, but Ga is the one with highest solubility for Si (see table 3.4). Between room temperature and 100 °C the solubility of Si in Ga ranges from 10^{-8} to 10^{-6}

atom% [1] and, although low, the solubility at 100 °C is comparable to the solubility in another ec-LLS system (Ge in Hg at room temperature [9]).

	Hg	**Ga**	**In**
Si solubility (atom%)	$< 4\text{x}10^{-11}$	$1.1\text{x}10^{-7}$	$1.9\text{x}10^{-16}$

Figure 3.4: Si solubility for different liquid metals extrapolated to 30 °C [9].

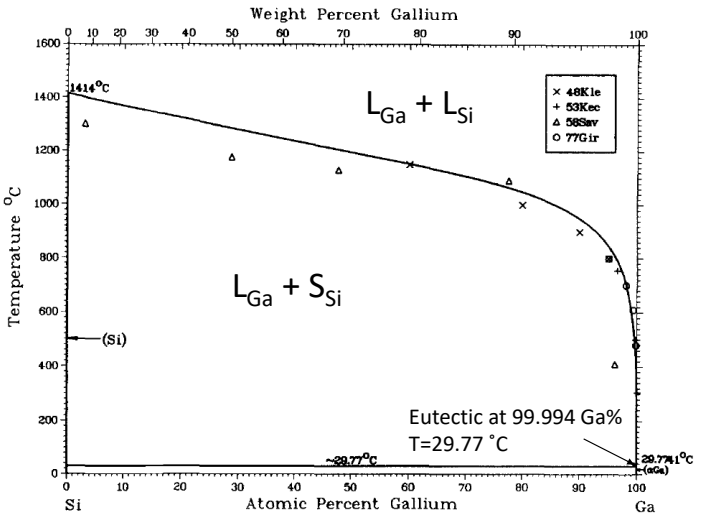

Figure 3.5: Si-Ga phase diagram. Adapted from [51].

Moreover looking at the phase diagram in fig. 3.5 is underlined the fact that Ga and Si can be eutectic at $\sim$ 30 °C, which means that potentially the Si-Ga solution can reach the supersaturation and precipitate in crystalline Si already at that temperature.

[1] Determined by extrapolations of published metallurgical data for the Ga-Si system [51].

CHAPTER 4

Fabrication process

In this chapter techniques and instruments used for the electrochemical fabrication of Si nanostructures (NS) will be presented. The standard operating procedure (SOP) for this process is reported in the appendix. As shown in chapter 1 it is possible to obtain NS in many different ways. It has been chosen to use electrochemistry combined with the properties of Ga as catalyst because this technique best fits the purpose of this work, which is obtaining nanostructures suitable for photovoltaic (PV) application in a simple, cheap and effective way.

4.1 Solution

As explained in section 2.3 an electrochemical solution consists of a solvent and an electrolyte, where the electrolyte consists of a supporting electrolyte to enhance the conductivity, and a precursor that provides the ions of the element to be deposited. For the growth of silicon nanostructures, a precursor containing Si is therefore required.
According to literature, the chemicals listed in table 4.1 are the most commonly used for Si electrodeposition [52]. It is also important to consider that most of the Si precursors react with water, which means that Si must be deposited from a non-aqueous medium and under an inert gas atmosphere (as ambient air contains enough water to drive this reaction).

After a deep evaluation of different works on Si electrodeposition the following solution has been chosen:

$$PC + TEAC + SiCl_4, \tag{4.1}$$

where PC stands for propylene carbonate and TEAC for tetraethylammonium chloride. The concentration of TEAC has been fixed at 0.2M and the concentration of $SiCl_4$ at 0.5M.

Solvents	Supporting electrolytes	Precursors
anhydrous propylene carbonate (PC)	tetraethylammonium chloride (TEAC)	$SiCl_4$
tetrahydrofuran (THF)	tetrapropylammonium chloride (TPAC)	$SiBr_4$
acetonitrile (AN)	tetrabutylammonium chloride (TBAC)	
dimethyl sulfide		
1-methyl naphtalene (1-MN)		

Table 4.1: Common chemicals used in Si electrodeposition [52].

$SiCl_4$ is by far the most commonly Si precursor used in literature [12][52][53][45][54][8] and therefore has been preferred to $SiBr_4$, although they have very similar properties. Propylene carbonate, instead, is the safer one between the solvents. All the supporting electrolytes are basically equivalent because the chloride ion is the dominant current carrier, so it has been decided to start using TEAC. Of course would be interesting for future works to try to change the supporting electrolyte and its concentration. More detailed informations about these chemicals can be found in the appendix (table 8.1).

Ist is important to point out that $SiCl_4$ reacts with water in an exothermic vigorous reaction releasing a toxic gas (HCl):

$$SiCl_{4(l)} + 2H_2O_{(l)} \rightarrow SiO_{2(s)} + 4HCl_{(g)} \tag{4.2}$$

this means that $SiCl_4$ or any solution containing this compound must be always handled under a water-free environment (i.e. nitrogen or argon glovebox). Moreover $SiCl_4$ boiling point is ∼57 ℃, so a backpressure to overcome the volatility can be needed depending on the temperature of the experiment.

4.1.1 Preparation of the solution

Because of the $SiCl_4$ reactivity with water the solution has to be prepared in a water-free environment and all the chemicals involved have to be stored there, in the case of this work has been used a MBRAUN LABstar Nitrogen glovebox (fig. 4.1). Since $SiCl_4$ can poison the catalyst that removes oxygen from the glovebox, it is necessary to turn off the circulation of the glovebox and start the purging process when using this chemical. All the solution preparation is done in the glovebox. After removal of the solution, the glovebox has to be purged for some hours before turning on the circulation again.

It's also necessary to prepare a solution without $SiCl_4$ in order to use it for reference measurements. This solution could be actually prepared under normal atmosphere, but it has been

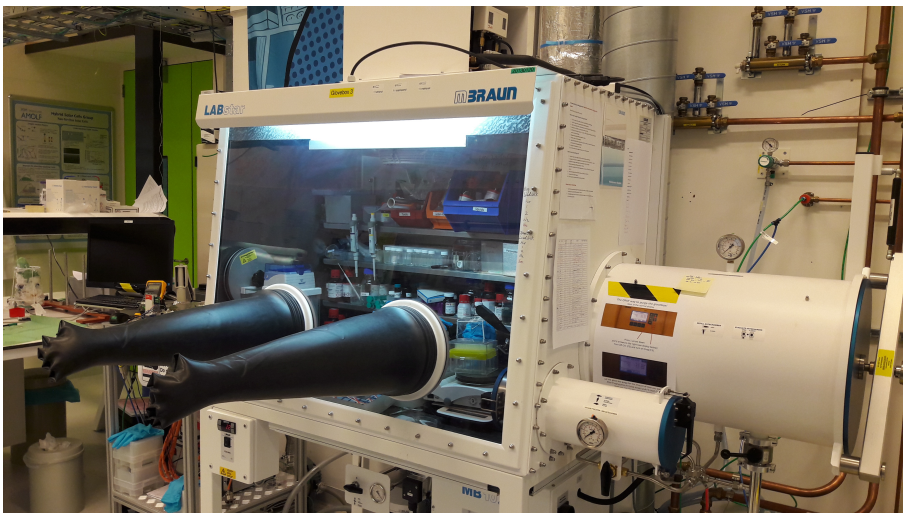

Figure 4.1: MBRAUN LABstar Nitrogen glovebox

chosen to keep the same conditions for both the processes.
The preparation of the solution with the desired molarity of precursor and supporting electrolyte requires some calculations. Here are listed the needed properties of $SiCl_4$ and TEAC [55]:

$SiCl_4$ molecular weight (MW_{SiCl_4}): 169.9 g/mol
$SiCl_4$ density (ρ_{SiCl_4}): 1.483 g/ml
TEAC molecular weight (MW_{TEAC}) = 165.7 g/mol

With these informations it is easy to calculate the desired amount of chemicals, in grams for TEAC (A_g) and in ml for $SiCl_4$ (A_{ml}). If M_{SiCl_4} [mol/l] is the desired molarity of $SiCl_4$, M_{TEAC} [mol/l] the desired molarity of TEAC, n the number of moles and V [l] the volume of the solvent, then the amount of chemicals for a particular molarity M and solvent amount V is given by:

Amount of $SiCl_4$:

$$A_{ml} = \frac{A_g}{\rho_{SiCl_4}} \text{ [ml]}$$
$$A_g = n \cdot MW_{SiCl_4} \text{ [g]}$$
$$n = M_{SiCl_4} \cdot V \text{ [mol]}$$

Amount of TEAC:

$$A_g = n \cdot MW_{TEAC} \text{ [g]}$$
$$n = M_{TEAC} \cdot V \text{ [mol]}$$

4.2 Cell design

As already stressed, the solution involved in the experiment reacts with water, therefore the electrochemical cell has to be properly sealed in order to avoid contact with air's moisture. For

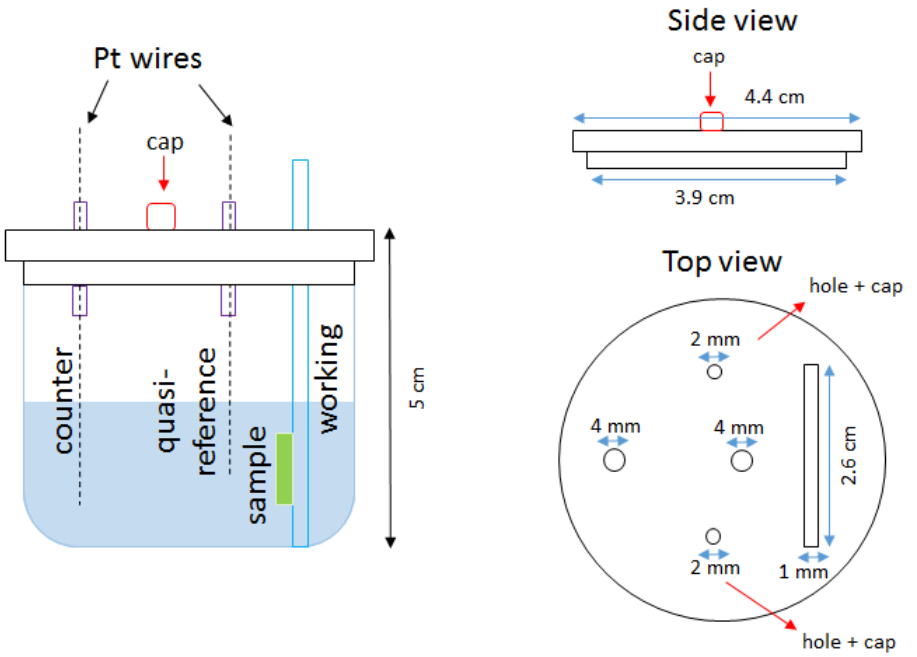

Figure 4.2: Schematic of the cell design with top and side view of the cover.

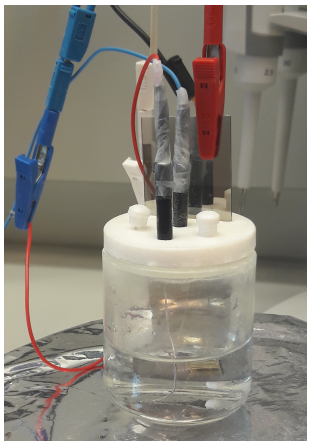

Figure 4.3: Actual cell used in the experiment.

this reason a cell with the required characteristics has been designed and built (fig. 4.2 and 4.3).

The cell has a borosilicate glass body, obtained by cutting the top a beaker, while the cover is made of teflon and has been custom-built in order to fit exactly with the diameter of the body. In the cover there are also a rectangular aperture with the dimensions of a common microscope slide and four holes: the two biggest holes are used to insert the counter and quasi-reference electrodes, which consist of Pt wires connected to standard electrical wires in the way explained in fig. 4.4. The two other holes are closed by air-tight teflon caps and can be used for different purposes, such as fill the cell with the solution or insert a thermometer.

The sample (i.e. the working electrode) is glued to a microscope slide sputtered with Ti in order to make it conductive. Different glues were tested in order to assess their chemical resistivity to the used chemicals and a common glue from Velpon has been chosen. When Si substrates were employed an eutectic solution of In and Ga was added on the back part before gluing them to the slide, in order to obtain an ohmic contact. The slide with the sample is then inserted in the rectangular aperture.

This cell design is simple but effective for the experiment, indeed it allows to easily and quickly change sample, substitute the Pt wires if damaged and add a stirring magnet if desired, in addition to the advantage of having the chance to check constantly by eye the development of an experiment.

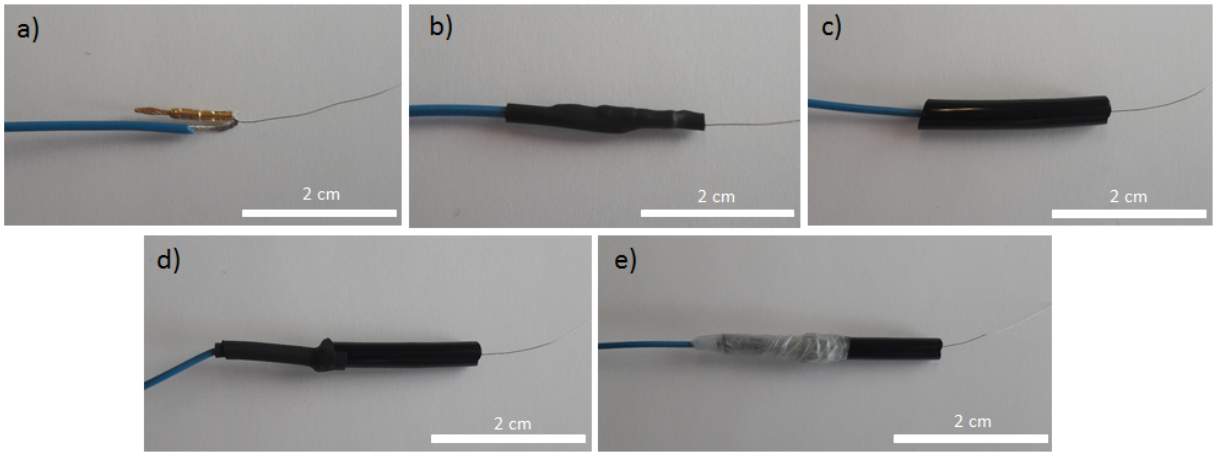

Figure 4.4: Set up of the electrical connections: a) The Pt wire and the standard wire are inserted in the metallic tube, which then is pressed to fix them. One of the wires has to be bended towards the opposite direction. b) A shrinking tube is employed to surround the central part, so that, once heated, keep everything in the proper position. Other shrinking tube can be added over the previous one if needed so that the whole connection can fit tightly in a plastic tube with a diameter of 3 mm. c) The connection is inserted in a plastic tube with 3 mm internal diameter and 4 mm external diameter. At this point the connection is ready to be inserted in the cover of the cell, but some small improvement are useful to make it more air-tight: d) the extremity of the tube outside the cell is again surrounded with a shrinking tube and properly heated. e) Some parafilm is finally used to cover everything.

4.2.1 Sputtering

As mentioned in the previous section, the slide used as support for the sample has been covered by a 50 nm layer of Ti in order to make it conductive. Ti has been chosen between the available conductive materials because is not etched by gaseous $SiCl_4$, that can be released inside the cell for temperatures above $SiCl_4$ boiling point. The layer has been deposited using a Magnetron Sputter Coater Leica EM ACE600.

Magnetron sputter coating is performed using ionized argon to create a plasma: the argon ions are accelerated by high voltage and directed towards the source via a magnet, there they collide with the target and displace surface atoms, which are then driven by diffusion towards the area below the target and coat the sample. During the sputtering the chamber with the samples and the target is under vacuum ($\sim 10^{-3}$ mbar). Argon is used to create the plasma for target erosion because it is inert and doesn't react either with the target or with the growing layer.

A scheme of Magnetron Sputtering system is presented in fig. 4.5, where is showed a single-target sputtering system. The one used in this work has two target holders and each of them can ignite and confine its own plasma, therefore multi-layer deposition is possible by sputtering consecutively different metals, but at most two elements can be deposited in the same process. In any case in this work only one target has been employed.

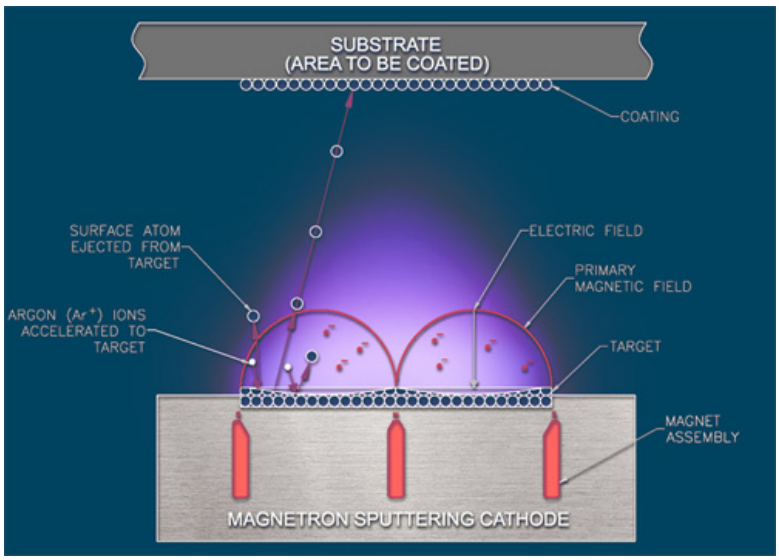

Figure 4.5: Magnetron Sputtering system

4.3 Ga deposition

One of the things at the basis of this work is the fact of using Ga seeds as catalyst for the growth of Si nanostructures. It is known that Ga nanoparticles can be obtained with several methods, for example self-assembly during molecular beam epitaxy (MBE) [56][57], optically regulated self-assembly [58], colloidal synthesis [59] or thermal evaporation [60].
The method used in this work is the thermal evaporation, this technique is indeed quite quick and doesn't involve many different steps, unlike for example the optically regulated self-assembly or the colloidal synthesis.

In fig. 4.6 is shown a standard thermal evaporator system: during the deposition the system

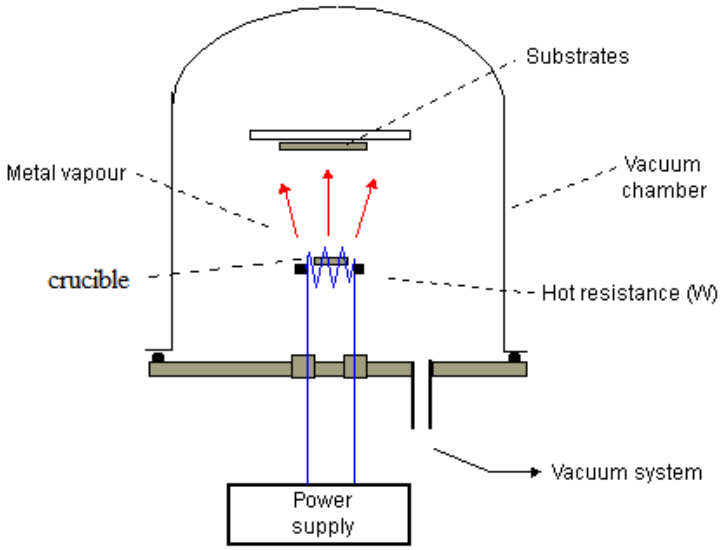

Figure 4.6: Thermal evaporator system.

is under high vacuum ($\sim 10^{-6}$ mbar), a crucible with the metal to be deposited is placed on the top of a resistance which is heated through the passage of current by Joule effect, after some time the metal evaporate and the particles diffuse towards the substrate placed on the top of the chamber and facing downwards, where they condense back to a solid state. Thanks to the vacuum the evaporated particles can travel directly to the deposition target without colliding with the background gas, which can reduce the amount of metal vapor that reaches the substrate and it makes the deposition thickness difficult to control.
In the case of this work the metal to be deposited is Ga, whose melting point is 29.77 °C. Therefore the Ga containing bottle has to be heated for a while in a water bath and, when the metal is melted, is then possible to use a syringe to fill the crucible in the evaporator with a proper amount of Ga. To deposit Ga on the surface of the substrate has been used a home-built thermal evaporator dedicated to the evaporation of materials which can contaminate the system during the process, such as Ga or Sn.
During the deposition, the Ga self-assembles in nanodroplets because of surface diffusion and Ostwald ripening. In fig. 4.7 and 4.8 is showed the aspect of a Si substrate after Ga deposition.

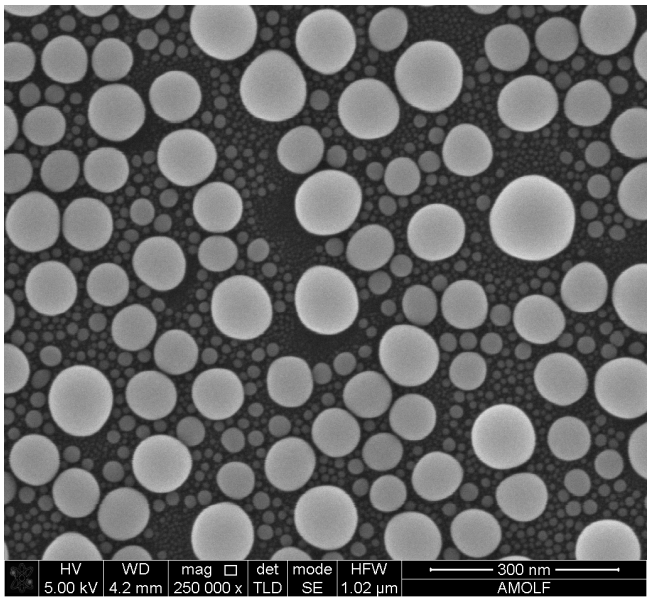

Figure 4.7: Ga deposition on Si substrate - top view.

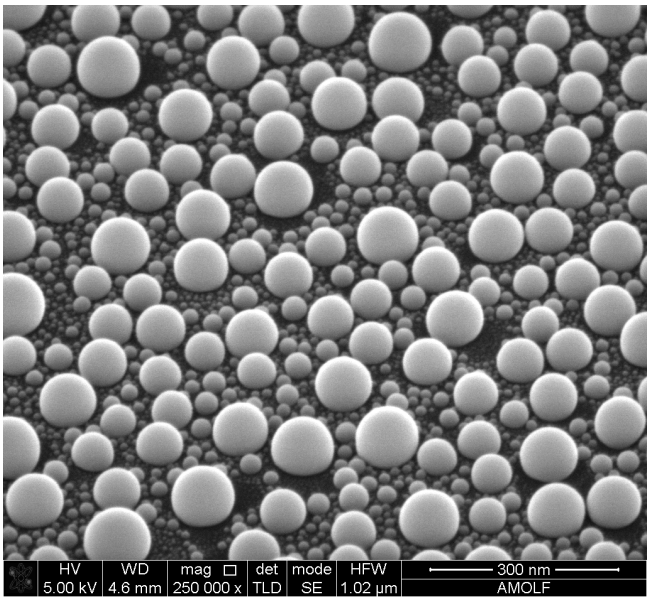

Figure 4.8: Ga deposition on Si substrate - tilted view.

4.4 Electrodeposition

The reactions and the process involved in the electrodeposition have already been exposed in section 3.1. From the practical point of view every experiment requires some preparation.
First of all, it is possible to have a theoretical estimate of the height of the deposition based

on the parameter chosen for limiting the deposition. This estimate is based on the assumption that all the current is due to the reduction reaction of the Si ions and all the related charge is depositing. Moreover the calculated height is referred to the deposition of a layer. These assumptions are not entirely satisfied, but the calculation permits anyway to have an idea of the amount of deposition and to choose the parameters which limit the deposition consequently.

For the following calculation the listed Si physical properties are considered [61]:

Lattice constant (a): 0.5431 nm
Number of atoms in 1 cm^3 *(*N_V*)*: $5 \cdot 10^{22}$ cm^{-3}
Electronic charge (q) = 1.603·10^{-19} C

From the volumetric density and lattice parameters, one can assess the surface density to be N_S=$2.72 \cdot 10^{15}$ cm^{-2}.

Given the total charge Q [C] that is deposited during the experiment and the area A [cm^2] of the substrate (i.e. WE), is possible to predict the height h [nm] of the deposition through the following steps:

1. *Number of electrons* $\#e^- = \dfrac{Q}{q}$
2. *Number of Si atoms* $\#Si = \dfrac{\#e^-}{4}$
3. *Number of monolayers* $\#ML = \dfrac{\#Si}{N_S \cdot A}$
4. *Deposition height* $h = \#ML \cdot a$ [nm]

If instead of the charge are given the current I and the time t of the deposition, equation 1. has to be replaced with:

1. *Number of electrons* $\#e^- = \dfrac{I \cdot t}{4 \cdot q}$

Of course is also easily possible to invert the calculation and get the charge or the current necessary for obtaining a certain height of deposition.

Once chosen the parameters of the deposition with the help of these calculations it is possible to proceed with the experiment itself. The sample is glued to a Ti coated microscope slide and mounted in the cell together with the electrodes. Then, inside the glovebox, the cell is filled with the solution[1] and sealed.
Once back in the hood, working, counter and quasi-reference electrodes have to be properly connected to the potentiostat[2]. To perform the experiment at a certain temperature (higher than room temperature) the cell has to be put in a water bath placed on an hot plate set with the desired temperature, a thermometer is also inserted in the bath so that is possible to measure the actual temperature of the system.
After the experiment the cell is transferred back to the glovebox, there it is opened and the sample is removed from the slide, cleaned properly with PC and transported to the hood in a beaker filled with PC. Here it is cleaned again with isopropanol (IPA) and deionized water, dried with N_2 and stored. The cell itself is also cleaned after each experiment with IPA or acetone and water, and then dried with N_2.
Since $SiCl_4$ is reacting with water an important point is the waste disposal: every $SiCl_4$ containing waste has to be neutralized in order to avoid the evolving of HCl gas in case of accidental contact between the waste itself and water. To neutralize the solution a vessel containing room temperature water has to be prepared with volume 5-10 times that of the solution. The solution is slowly poured in the vessel while stirring, so that the HCl gas can evolve and flow in the hood. After around 20 minutes of stirring the solution in the vessel is neutralized and can be poured into the waste bin for organic acids.

[1] In general the amount of solution used for each experiment has been between 10 ml and 15 ml, enough for the sample to be completely soaked, moreover a stirring magnet can be add in the cell in order to improve the ions' movement during the experiment.

[2] The potentiostat employed in this work is Bio-Logic SAS SP-200.

CHAPTER 5

Characterization Techniques

In this chapter will be described the different instruments and techniques employed for the characterization of the deposited material. For assessing the morphology of the deposition the main technique has been the Scanning Electron Microscope (SEM), while for identifying the chemical composition of the grown material have been used both Energy-Dispersive X-ray spectroscopy (EDX) and X-ray Photoelectron Spectroscopy (XPS), this last technique could also provide information about the oxidation level of the deposition.
Has been tried to analyze the deposited material also through Raman spectroscopy (WiTec system) and X-Ray Diffraction (XRD), but has not been possible to obtain any useful information from those measurements.

5.1 Scanning Electron Microscope (SEM)

A scanning electron microscope (SEM) [62][63] is a type of electron microscope which produces images of the surface of a sample by scanning it with a beam of electrons previously focused. The electron beam interacts with the atoms of the sample at various depths producing different signals (fig. 5.1), for example secondary electrons (SE), reflected or back-scattered electrons (BSE), characteristic X-rays and light (cathodoluminescence) (CL), auger electrons (AE) and transmitted electrons. Those signals are collected by detectors and converted into another signal that is sent to a screen similar to a television screen, which produces the final image. In general a single SEM doesn't have detectors for all the described signals, although the standard equipment includes always a secondary electrons detector.

Fig. 5.2 represents schematically how a typical SEM works. The process is happening under vacuum (generally high vacuum) so that electrons can be emitted and have no other interaction than with the sample.
The electron beam is generated from an electron gun, which can be a thermionic gun or a

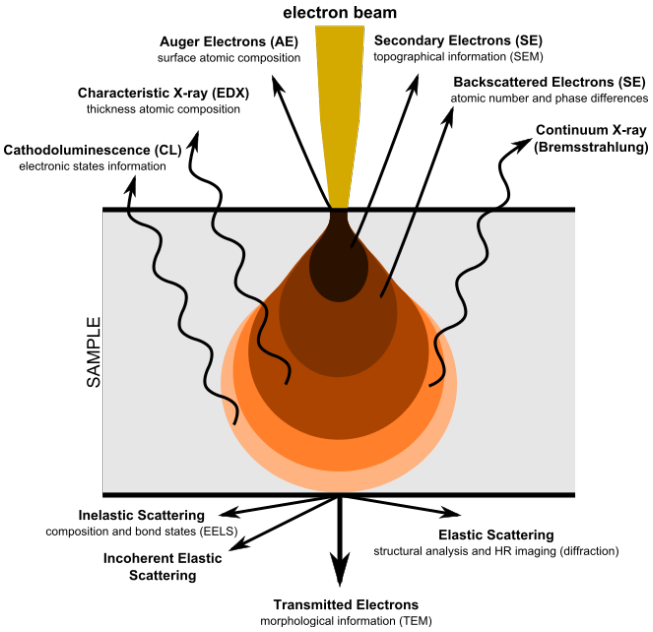

Figure 5.1: Signals derived by the interaction of the electron beam with the sample.

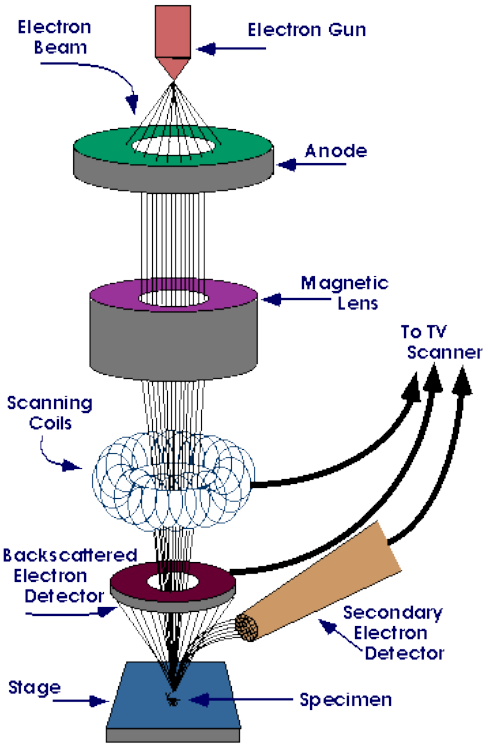

Figure 5.2: Schematic of a SEM.

field emission gun (FEG). In the first case there's a filament, typically made of tungsten or LaB_6, which is heated releasing electrons because of thermionic emission. The field emission guns instead use a strong electric field to extract electrons from the filament, these guns (called Schottky emitters) are more expensive and require ultra high vacuum, but in many aspects they are preferable (for example brightness, monochromaticity, lifetime).

The electron beam pass then through a series of electromagnetic lenses which focus it onto the stage, where the sample is placed. Another essential component are the scanning coils, indeed the images are produced by sweeping the electron beam in a tv-like raster on the sample while displaying the detected signals from the electron detectors. This sweeping movement is provided by the scanning coils.

The samples in a SEM are usually fixed to a stub consisting of a metal disc, which is mounted on the stage mechanism that allows the linear x, y, z movements and rotations around a vertical and a horizontal axis. X and y movements permit to move on different areas of the sample, while the z movements help to find the surface of the specimen and focus. Nonconductive samples collect charge when scanned by the electron beam and this causes scanning faults and other image artifacts. This is why for conventional imaging in the SEM specimens should be electrically conductive, at least at the surface, and non-conducting materials are usually coated with an ultrathin coating of electrically conducting material.

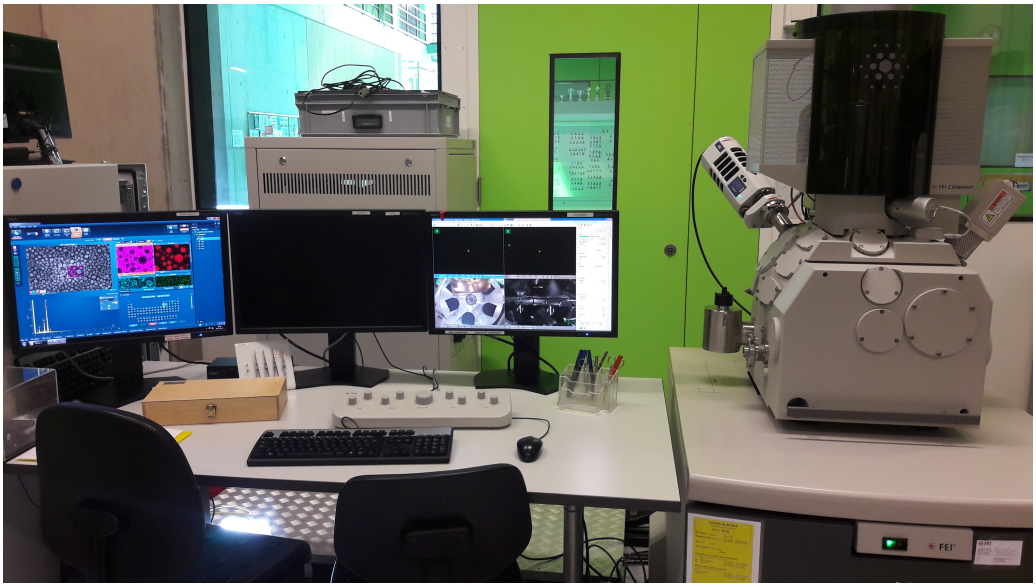

Figure 5.3: FEI Verios460 XHR SEM employed in this work. Since it is provided with a X-ray detector, also the EDX analysis has been performed with this instrument.

The SEM employed for this work (fig. 5.3) is the FEI Verios460 XHR (extreme high resolution), it provides sub-nanometer resolution from 1 to 30 kV and enhanced contrast, moreover allows ultra-high resolution imaging at low energy on insulating samples with no conductive coating. It is provided with a Schottky electron gun which can deliver a low energy spread beam (< 0.2 eV). It is possible to image in *field-free mode*, which is the basic mode present in all the SEM, or in *immersion mode*, in this case an immersion lens and an high magnetic field (~ 1.5T) are used to obtain ultra high resolution imaging. The navigation on the sample is simplified by a NavCam system.

5.2 Energy-Dispersive X-ray spectroscopy (EDX)

Energy-dispersive x-ray spectroscopy (EDX) [63][64] is an analytical technique used for the elemental analysis or chemical characterization of a sample. The EDX analysis is performed collecting the x-rays released by the sample as consequence of the interaction with a high energy electron beam, therefore in general this analysis is carried out in combination with a SEM.
When the electron beam hits the sample, there is a high probability that an x-ray is generated. Indeed when an electron (from the beam) strikes an atom (in the sample) an electron originally positioned in an inner shell is ejected and to return to its lowest energy state the atom fill this "vacancy" moving an electron from a higher-energy shell. In doing so, this high-energy electron must release some of its energy in the form of x-rays and this energy is exactly equal to the

energy difference between the two levels. The resulting x-ray escapes the sample and hits the detector, which creates a charge pulse in the detector. This short-lived current is then converted into a voltage pulse with an amplitude reflecting the energy of the detected x-ray. Finally, this voltage pulse is converted to a digital signal and one more count is added to the corresponding energy channel. Once the measurement is completed, the accumulated counts produce a typical x-ray spectrum with the major peaks superimposed on the background, allowing to identify the chemical composition of the sample.
As the atomic structure of each element is different, it follows that, when stimulated, each element emits a specific pattern of x-rays, which can be separated according to the energy levels because the detector consists of a energy-dispersive spectrometer. Using a process known as x-ray mapping, information about the elemental composition of a sample can then be overlaid on top of the magnified image of the sample. Another characteristic which makes EDX particularly useful is that the amount of x-rays emitted by each element is related directly with the concentration of that element (mass or atomic fraction within the probing volume). This is why it is possible to convert the x-ray measurements into a final x-ray spectrum and assess the concentrations of the various chemicals present in a sample.
All elements except hydrogen and helium produce characteristic x-rays. Practical restrictions concerning a minimum energy level usually exclude the measurement of lithium (0.052 keV), but all other elements can be assessed simultaneously. Electron beams in the range of 100 eV to 20 keV are readily measured with a Si(Li) or SDD detector, and this range can be extended to 100 keV with an HpGe detector. This approach enables access to virtually the entire periodic table (except H, He and Li) and it is a great practical value of EDX.
In the case of this work the EDX is incorporated in the SEM described in the previous section.

5.3 X-ray Photoelectron Spectroscopy (XPS)

X-ray photoelectron spectroscopy (XPS) [65][66] is a surface-sensitive spectroscopic technique that allows to determine the binding energy of the elements on the surface (0.5-3 nm) of a sample and therefore assess its chemical composition and electronic and chemical state, so for example is possible to determine the different oxidation levels of the material.

The sample is irradiated with a focused beam of x-rays, the incident photons interact with the surface through photoelectric effect releasing electrons, which kinetic energy is measured allowing to determine their binding energy E_B according to the equation:

$$E_B = h\upsilon - E_k - \Phi \tag{5.1}$$

where $h\upsilon$ the energy of the incident photons, E_K the kinetic energy of the electron and Φ is the work function of the spectrometer.

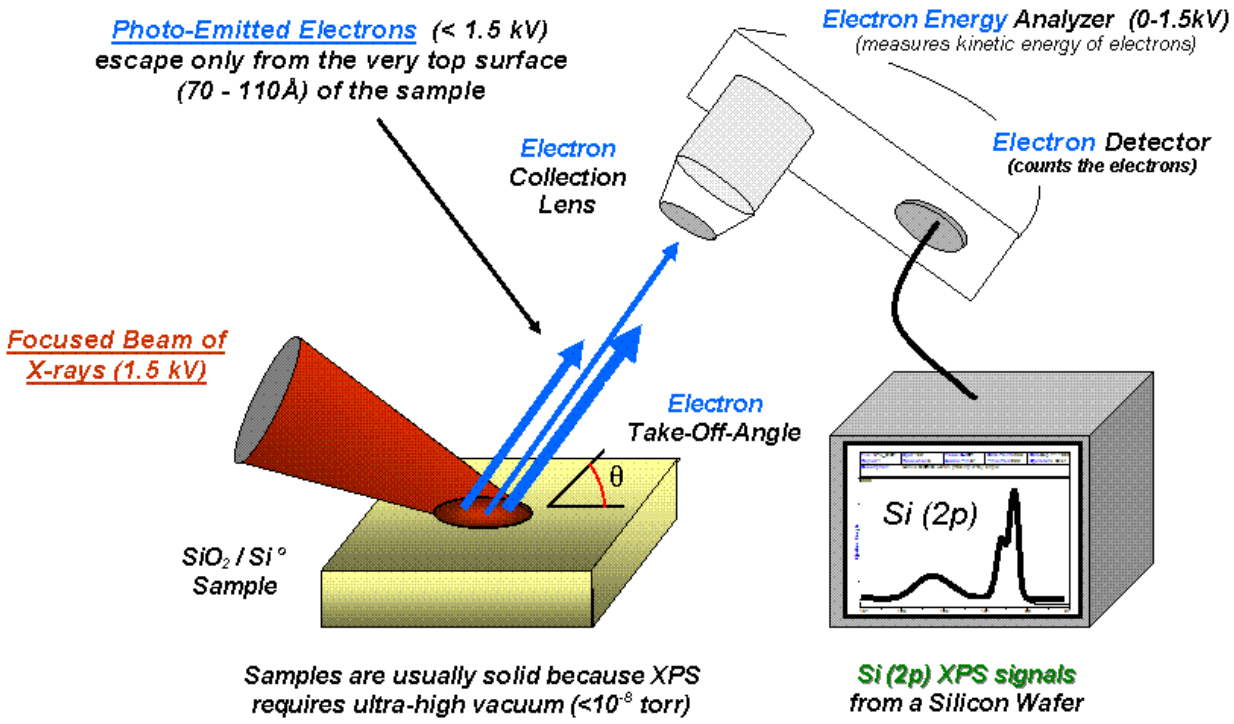

Figure 5.4: Scheme representing the components of a standard XPS system measuring a Si wafer.

The photoelectrons are then collected by an hemispherical analyzer, which consists of two concentric hemispheres with different potentials, in this way the incoming electrons are forced to a circular orbit which radius depends on its energy. The analyzer is therefore separating the electrons according to the energy, then they are directed towards the detector, where the signal is converted in digital. All the system is kept under high vacuum to avoid the scattering of the photoelectrons with other particles.
The result of a XPS measurement is a spectrum with peaks corresponding to the binding energies of the elements on the surface of the sample. Often there's a shift in the peak position due to the system itself. Before every experiment is therefore important to measure a reference sample of a known material in order to compare experimental and theoretical peaks and calculate the proper shift correction.

The measurements of this work has been performed with a setup (fig. 5.5) made up of a XM1200 monochromator for the x-ray source and a HiPP-3 analyzer, both from Scienta Omicron. The x-ray source for the monochromator has a single, static, water-cooled aluminum coated anode and two filaments of thoria-coated tungsten-rhenium with different focusing to give a small and larger electron spot on the anode. The emitted x-rays are Al K_α with energy E=1486.7 eV and

are focused by a quartz mirror to a diameter of $\sim$ 500 μm [67].The analyzer has a mean radius of 200mm and is provided with a 40 mm MCP detector monitored by FireWire (IEEE 1394) CCD-camera [68].

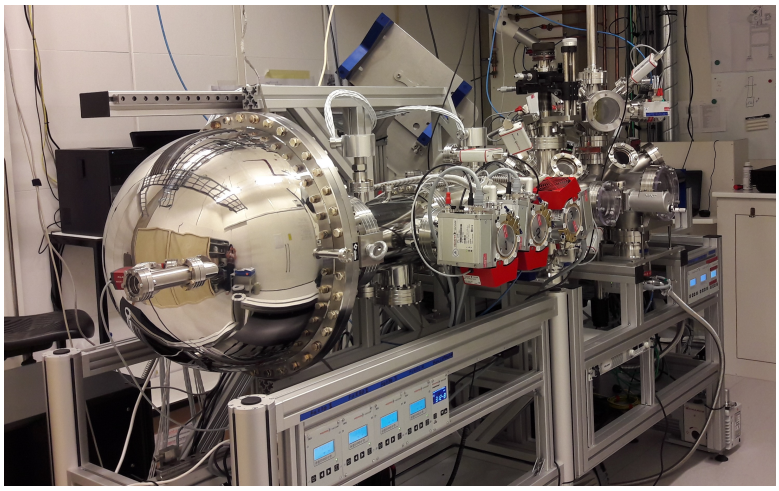

Figure 5.5: XPS setup employed in this work.

CHAPTER 6

Experimental results

In this chapter will be first exposed the results of the Ga evaporation required for the preparation of the samples and then the results of the electrodeposition experiments, divided by the effect of the different parameters on the deposition.
A table listing all the electrodeposition tests performed for each substrate is reported in the appendix (table 8.2).

6.1 Ga deposition

Before carrying out any electrodeposition experiment we prepared the substrate with evaporated Ga on the top. We have done some tests by changing the evaporation parameters with the aim of checking how much it is possible to control the characteristics of the deposition, such as dimensions of the droplets and density. Moreover Ga has been deposited on different substrates in order to assess how Ga is depositing on different materials and which are therefore the most suitable substrates for this work.
There are mainly two parameters which can be chosen for the evaporation: the rate of the deposition (by tuning the current) and the theoretical thickness of the deposition (assuming that it is a layer). The evaporation has therefore been done changing two different rates and two different thicknesses (see table 6.1). For these tests the substrate was Si.

	sample 1	**sample 2**	**sample 3**
rate (Å/s)	0.2	1.5	1.5
theoretical thickness(nm)	20	20	50

Table 6.1: Ga deposition parameters for three different tests on Si substrates.

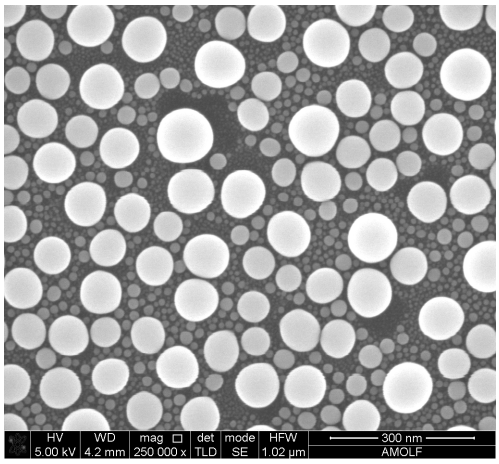

Figure 6.1: **sample 1** - SEM picture

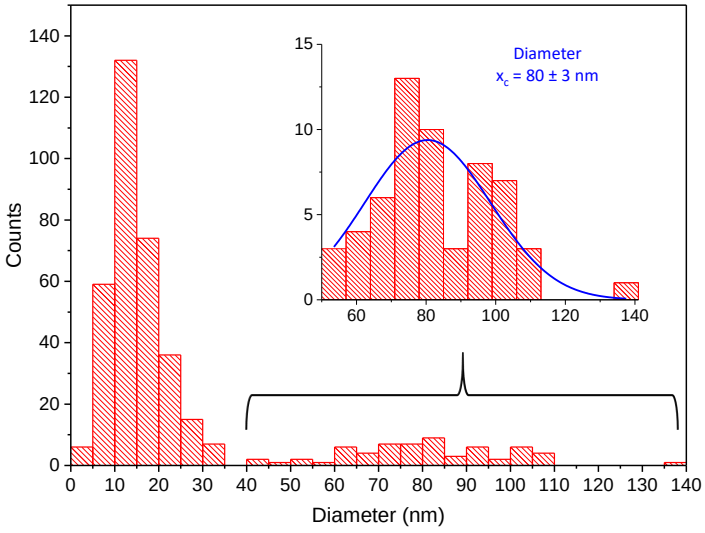

Figure 6.2: **sample 1** - diameters distribution

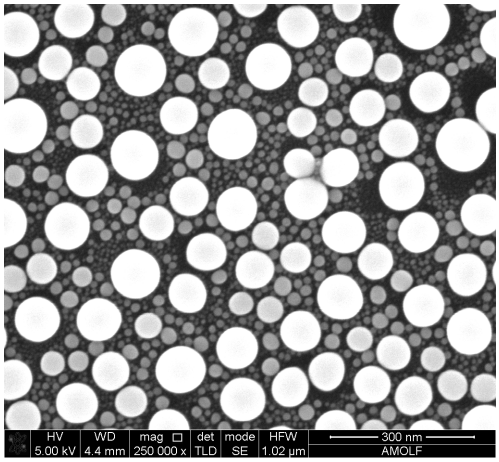

Figure 6.3: **sample 2** - SEM picture

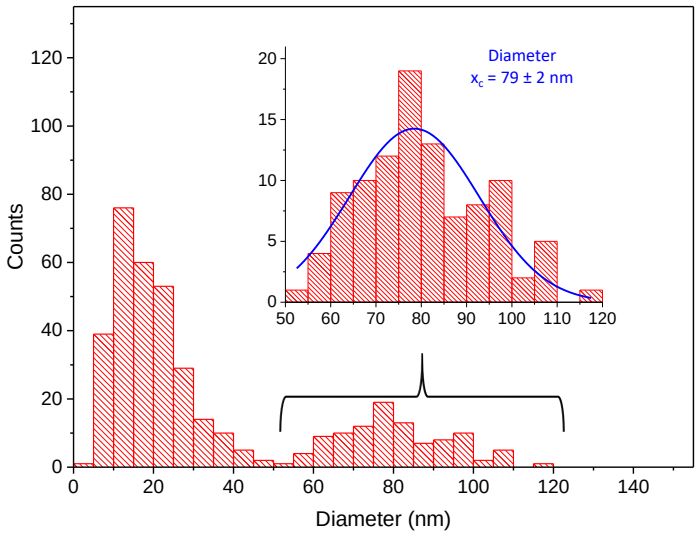

Figure 6.4: **sample 2** - diameters distribution

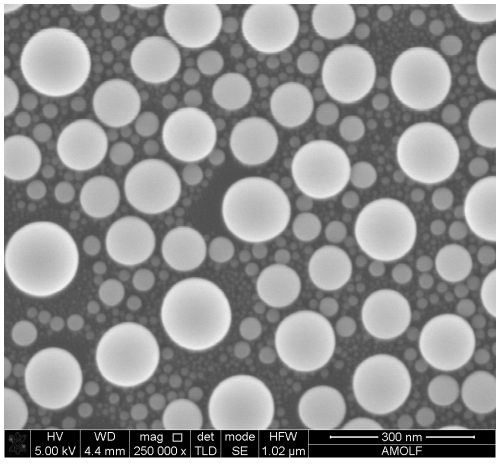

Figure 6.5: **sample 3** - SEM picture

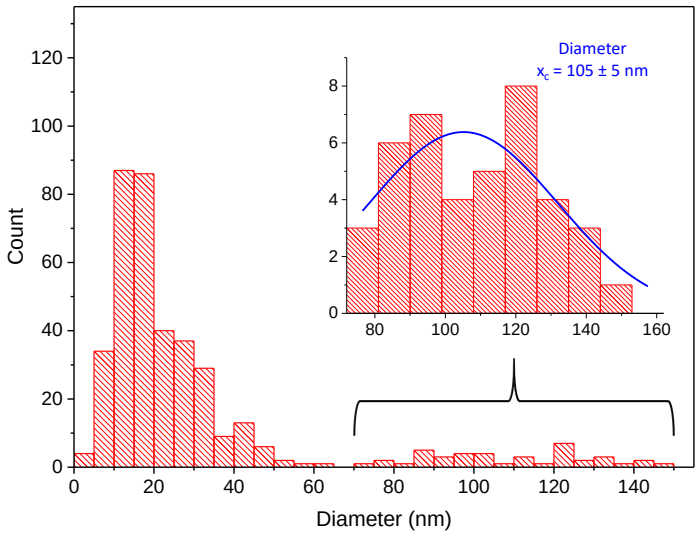

Figure 6.6: **sample 3** - diameters distribution

After the evaporation every sample has been checked with the SEM and the resulting picture has been analyzed through ImageJ with the aim of obtaining a rough statistic of the distribution of the droplets' diameters (fig. 6.1 - 6.6).
In each of the tests is evident that the diameters of the nanodroplets follow two distributions. Since during the evaporation the droplets are gathering because of diffusion and Ostwald ripening it is probable that the small droplets are just "residuals" which didn't gather in big droplets, which are of more interest for this work.
By comparing the histograms of the three samples it can be seen that the diameter of the droplets is only affected by the total nominal thickness and not by the rate of the deposition.
After these tests it was decided to fix the rate at 1.5 Å/s and the thickness at 25nm, so that the diameter of the big droplets is around 100 nm. These parameters have been kept for all the subsequent depositions.
After fixing the evaporation parameters tests have been performed to see how Ga is depositing on different substrates. Since the main requirement for a substrate that has to be employed as working electrode in an electrochemical experiment is to be conductive, there are many material that can be chosen. It has been decided to start with Si, stainless steel (SS), fluorine-doped tin oxide glass (FTO), Cu and Al.

In fig. 6.7 are presented the SEM pictures of the deposition on Si (a), SS (b), FTO (c),

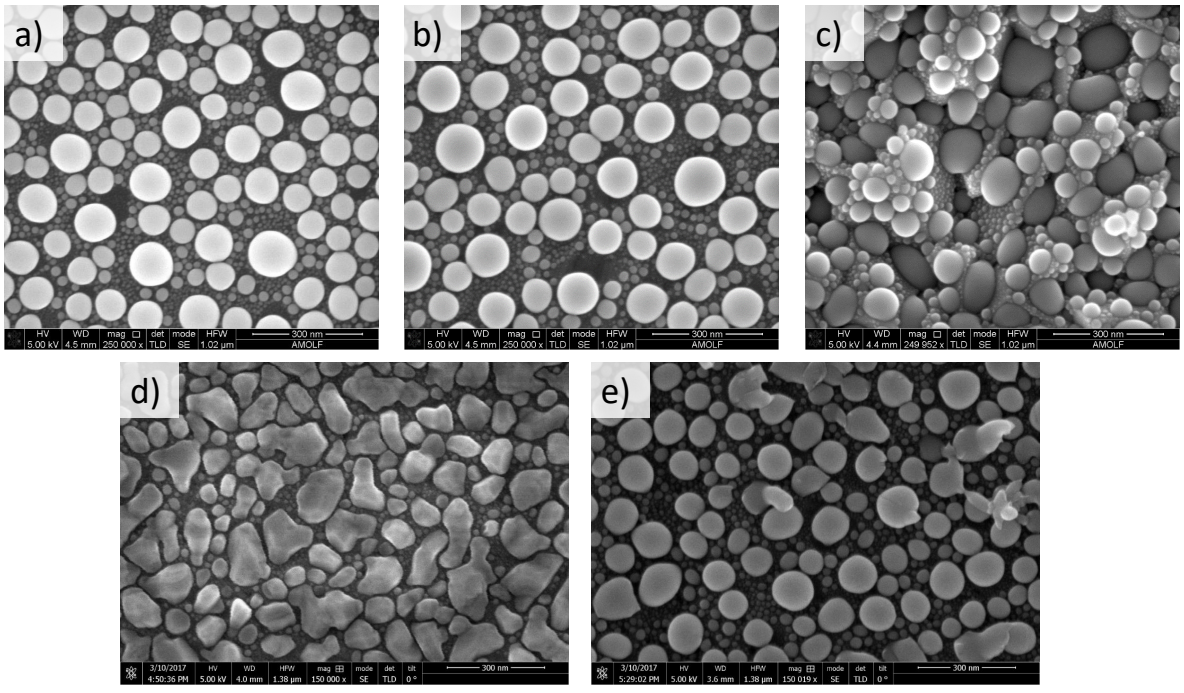

Figure 6.7: Ga deposition on different substrates: (a) Si, (b) stainless steel, (c) FTO, (d) Cu and (e) Al.

Cu (d) and Al (e). Si, SS and Al show very similar depositions, on FTO Ga is depositing in droplets as well, but they are heading to many different directions because of the roughness

of the surface. A different kind of deposition characterize instead the Cu substrate, looks like Ga alloyed with Cu and then re-crystallize, but, looking at the phase diagram [69], this is not something expected at the condition of the evaporation process. Nevertheless have been decided not to proceed with further experiments for explaining this behavior, but instead to focus on the substrates that yielded a high density of bigger droplets, as this is expected to aid the growth of silicon nanostructures.
What follows from these considerations is that, between the substrates which have been tested, the most suitable for the purpose of this work are Si, Al and SS, these have been therefore employed for the electrochemical tests.

6.2 Cyclic voltammetry on different substrates

Electrodeposition tests have been performed on all the substrates found suitable for the experiment (Al, Si and SS). In the next sections some of the depositions on these substrates will be shown, but first is important to obtain some qualitative information about the electrochemical process and how this can change depending on the substrate.

The graphs of fig. 6.8 represent all cyclic voltammetry (CV), therefore the voltage has been swept between two chosen potentials (in general between 0V vs EOC and -4V vs EOC, where EOC is the open circuit voltage, i.e. the equilibrium potential between the electrodes) in order to see how the current changes at the WE, the current has been then divided by the area of the sample to make the different measurements comparable.
From the voltammogram is possible to have an idea of the suitable voltages for the deposition. The shape of the curve can be related to many factors and is different every time, but what is sure is that as soon as a current is measured a reaction is happening in the solution. From the CV is not possible to know with certainty that "that" reaction is the Si reduction, but by comparing the curves obtained performing the CV with (blu, red and green curves) and without (black curve) $SiCl_4$ in the solution, is reasonable to make the assumption that "that" current is mainly related to the Si reduction. This brings to the conclusion that the most suitable voltages to apply for the deposition (i.e. the range of potentials which can be chosen to be fixed during a chronoamperometry) are those between the voltage at which a current appears and the voltage at which the reaction represented by the black curve starts. This is because it is desirable to avoid to involve in the deposition other reactions different from the Si reduction (this theme will be further deepen in section 6.4).
By comparing the CV in fig. 6.8 it can also be seen that, by changing the substrate, the same kind of CV curve (i.e. same temperature and CV parameters) seems shifted, therefore the range of voltages suitable for the deposition is slightly different depending on the substrate, but it remains more or less constant if the substrate is fixed and just the temperature is changed.
All the potentials employed for the depositions (and which will be mentioned in the next sec-

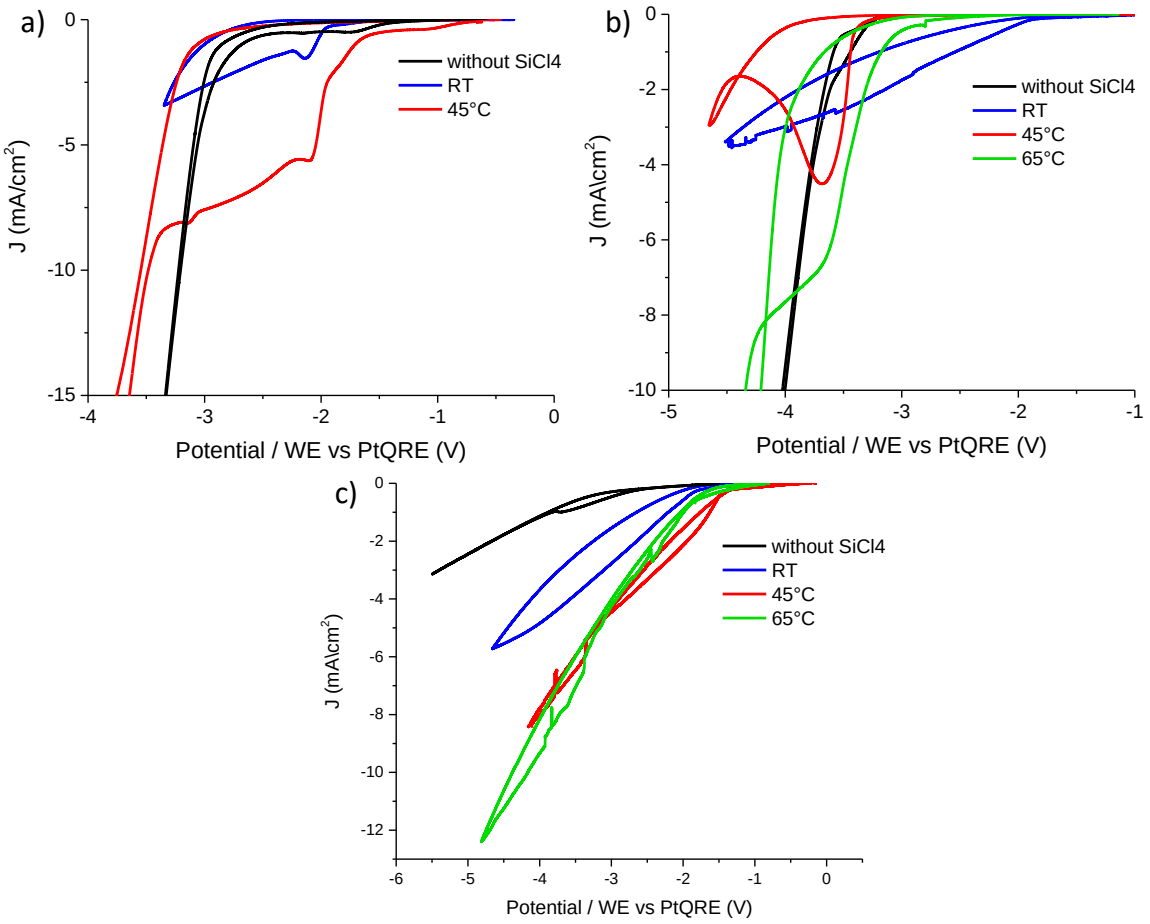

Figure 6.8: Cyclic voltammetry (CV) on different substrates and at different temperatures: (a) stainless steel substrate, (b) Aluminum substrate (c) Silicon substrate. All the substrate with evaporated Ga on the top. RT stands for room temperature.

tions) have been chosen according to these graphs.

6.3 The influence of temperature on the deposition

Electrodeposition tests have been performed at different temperatures and for different substrates. According to the Si-Ga phase diagram (fig. 3.5) already ∼30°C are enough for obtaining a solution of Si and Ga and consequently crystalline precipitation. The deposition has been performed also at room temperature (RT), although Ga is not expected to be liquid, in order to have a comparison. Going to higher temperatures than the Si-Ga eutectic point can be useful for obtaining bigger crystals or for having monocrystalline Si (instead of polycrystalline), because the mobility increases with temperature and there is higher concentration of Si at the supersaturation.

The samples have been characterized through SEM, EDX and XPS. During the experiments at

Sample	Temperature	Voltage (WEvsPtQRE)	Deposited charge
AlRT-1	RT	-2.5 V	0.03C
Al45-1	45°C	-3.6 V	0.03C
Al65-1	65°C	-3.6 V	0.03C

Table 6.2: Parameters for electrodeposition on Al+Ga substrate at different temperature.

a temperature different from RT the cell was placed in a water bath and the temperature was measured through a thermometer.

Al+Ga substrate

Electrodeposition has been performed on Al+Ga substrate at three different temperatures setting the amount of deposited charge as value at which stopping the chronoamperometry, the specific parameters are listed in table 6.2. Considering the dimensions of the samples and the deposited charge, and according to the calculations exposed in sec. 4.4, the expected thickness is $\sim$ 60nm.

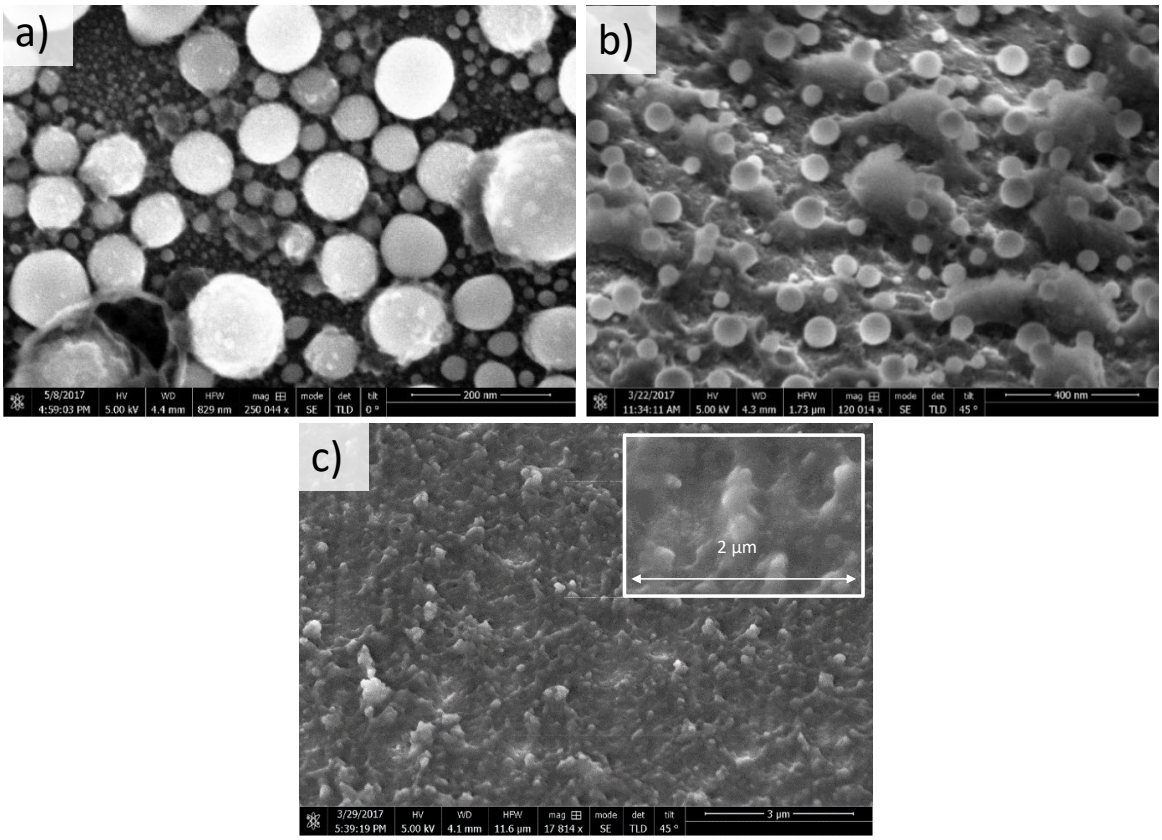

Figure 6.9: Si deposition on Al+Ga: (a) Room temperature, (b) 45°C, (c) 65°C. Pictures (b) and (c) taken with samples tilted at 45°.

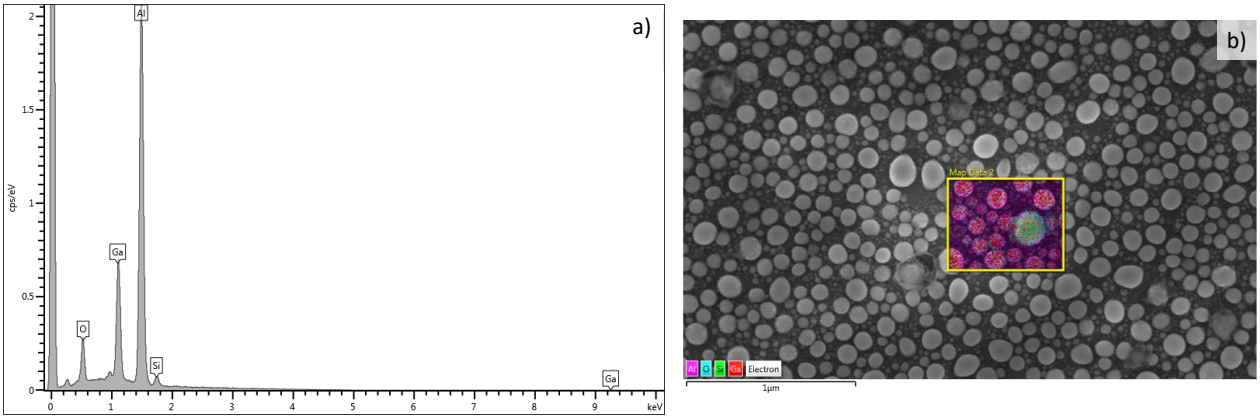

Figure 6.10: EDX analysis for electrodeposition on Al+Ga substrate at RT: (a) spectrum, (b) map.

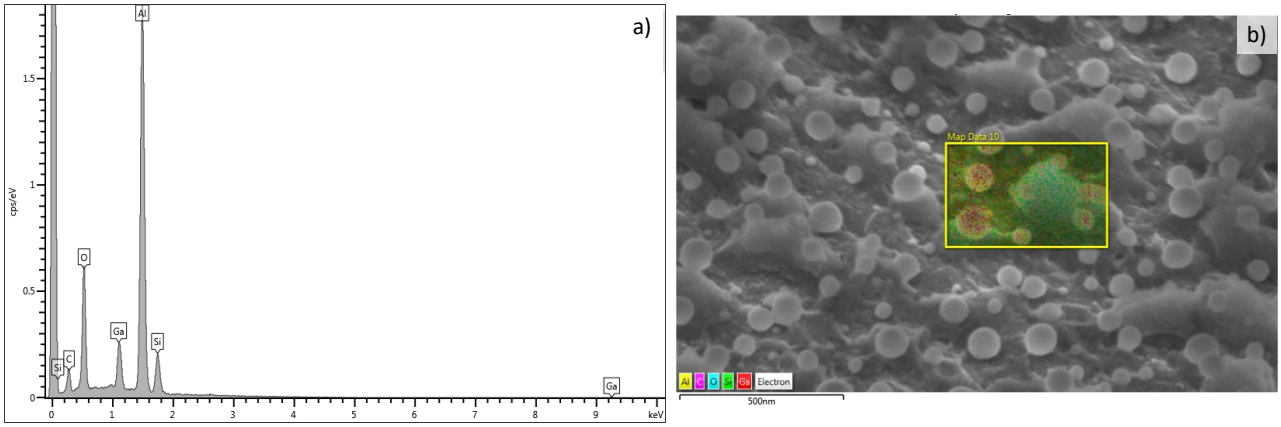

Figure 6.11: EDX analysis for electrodeposition on Al+Ga substrate at 45°C: (a) spectrum, (b) map.

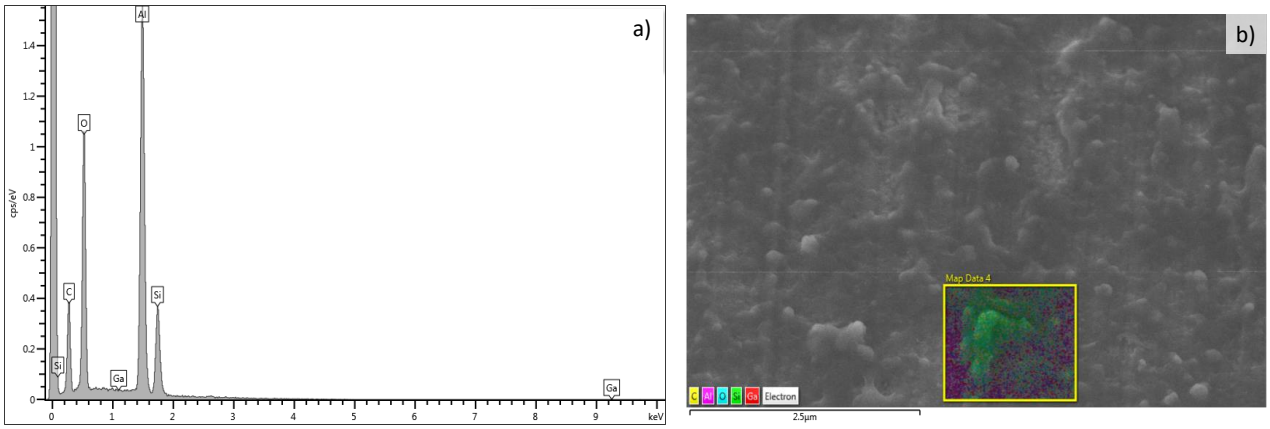

Figure 6.12: EDX analysis for electrodeposition on Al+Ga substrate at 65°C: (a) spectrum, (b) map.

Si oxidation state	Binding energy
Si	99.4 eV
Si_2O	100.4 eV
SiO	101.4 eV
Si_2O_3	102.5 eV
SiO_2	103.6 eV

Table 6.3: Theoretical values for the oxidation states of Si [72][70].

Temperature	Peak position
RT	100.30 ± 0.15 eV
45°C	103.26 ± 0.15 eV
65°C	103.66 ± 0.15 eV

Table 6.4: XPS peak position for deposition on Al+Ga substrate at room temperature, 45°C and 65°C.

The result has first been checked with the SEM (fig. 6.9). What is possible to assess directly from the picture is that the amount of deposited material is increasing with the temperature, despite the amount of deposited charge being constant in all the experiments. This is possible because the current registered at the WE (so the amount of charge) is not completely due to the reduction of Si ions, other processes involving the other elements of the solution can induce current. Therefore it seems that the lower the temperature is, the higher is the contribution to the current from solvent and electrolyte.

In the picture at RT (fig. 6.9a) the amount of deposition is very small and concentrated on the top of the biggest Ga droplets, while at 45°C the deposition is underneath Ga. This could mean that at 45°C Si actually enters the droplet and grew on the bottom, as expected, but for the moment is not possible to prove this statement. At 65°C, instead, the Ga droplets are no longer visible and the deposition is very rough.

To have a confirmation that the deposited material is Si the samples have been analyzed with EDX. From fig. 6.10 - 6.12 is indeed proved that the deposition in mainly Si, moreover the sample shows oxygen and trace of C. From the spectrum in fig. 6.12a is possible to see that there are no traces of Ga on the sample deposited at 65°C, the reason for this still has to be identified.

In order to better understand the quality of the deposition the sample have been also analyzed with the XPS, this technique allows to have informations about the oxidation state of the deposition and provides a further confirmation of the actual presence of Si.

The spectrum has been measured in the region of interest, which is around the binding energy of the Si(2p) peak (99.4 eV [70]), and calibrated according to the theoretical values of the $Ag3d_{5/2}$ and $Ag3d_{3/2}$ peaks[1]. The peaks have been fitted with either *Gaussian* or *Extreme function*[2], depending on the asymmetry level, and the error on the peak position is given by the error from the fit and a systematic error calculated from the peak shift obtained in repeated measurements.

The resulting peak positions are reported in table 6.4, while in table 6.3 the theoretical binding energies for the Si oxidation states are presented. The peaks are plotted in fig. 6.13 and

[1] $Ag3d_{5/2}$ = 368.3 eV, $Ag3d_{3/2}$ = 374 eV [71]

[2] $y = y_0 + Ae^{(-e^{-z}-z+1)} z = (x - x_c)/w$ where y_0 is the offset, A the amplitude, w the width e x_c the center.

lines have been drawn in correspondence with the theoretical peaks positions for the different oxidation states.

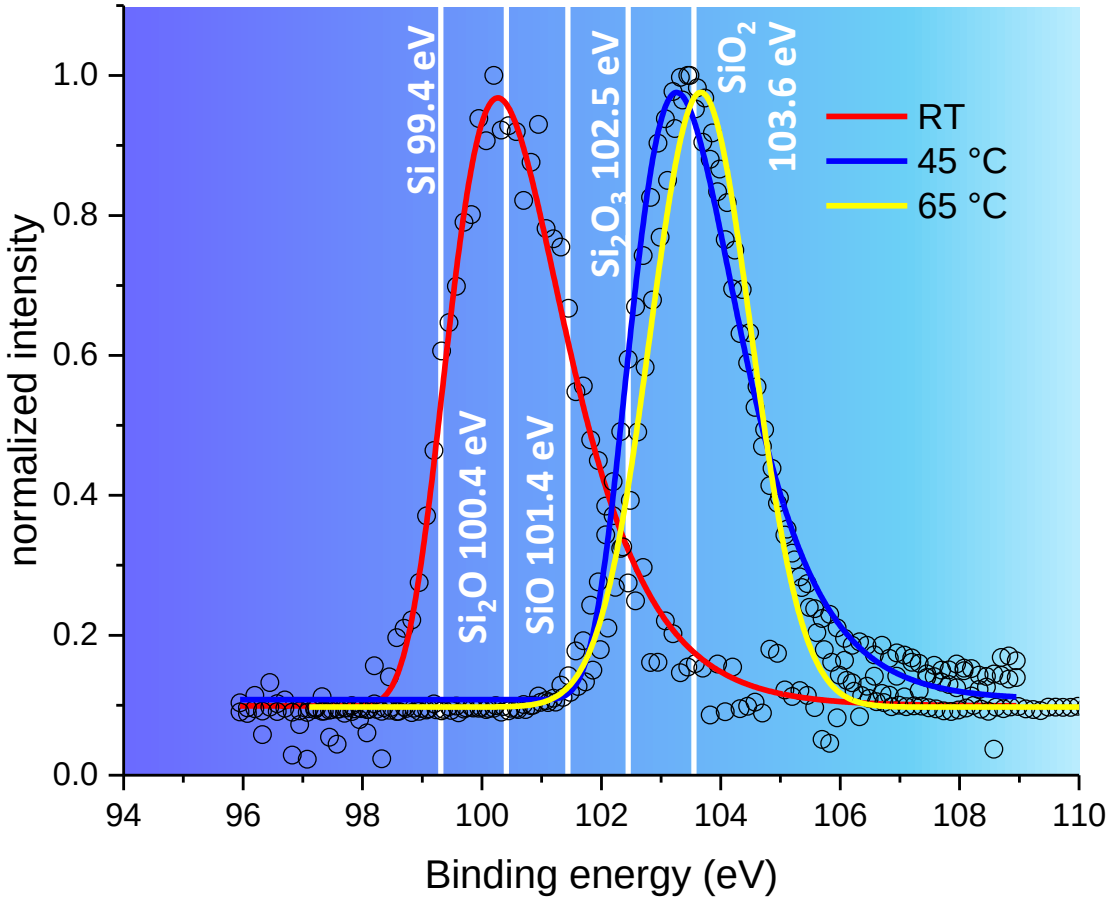

Figure 6.13: XPS peaks for deposition on Al+Ga substrate at room temperature (red), 45°C (blue) and 65°C (yellow). The white lines represent the energies of the different oxidation levels of Si. The intensity has been normalized since it is related to optimization processes performed independently for every sample.

From fig. 6.13 it is evident that the peak shifts in relation with the deposition temperature: the higher the temperature the higher is the oxidation degree of Si. In particular the deposition at room temperature shows a very low level of oxidation and it was the lowest found in this work. Since there shouldn't be oxygen in the solution and in the cell during the experiment, one hypothesis is that the as-fabricated samples oxidized upon removal from the cell and exposure to air. Nevertheless further experiments are needed to state if this is the actual source of the oxidation or if it is instead due to trace of oxygen in the solution. Regardless, the oxidation state can give information about the porosity of the grown material: looks like the higher is the temperature the more the deposited Si is porous.

Sample	Temperature	Voltage (WEvsPtQRE)	Deposited charge
SiRT-1	RT	-2.5 V	0.13C
Si45-1	45°C	-2 V	0.13C
Si65-1	65°C	-2.5 V	0.13C

Table 6.5: Parameters for electrodeposition on Si+Ga substrate at different temperature.

Si+Ga substrate

Electrodepositions with the same range of temperatures have been performed also on Si+Ga substrate with the idea that using a substrate of the same material of the deposition could help and improve the crystallization process. Since Si is a semiconductor, an eutectic solution of In and Ga has been added on the back side of the sample before placing it on the Ti coated slide to make an ohmic contact. Also in this case the chronoamperometry has been limited with the amount of deposited charge, but raised to 0.13C, in this way the expected thickness is ∼200nm. The parameters are listed in table 6.5.

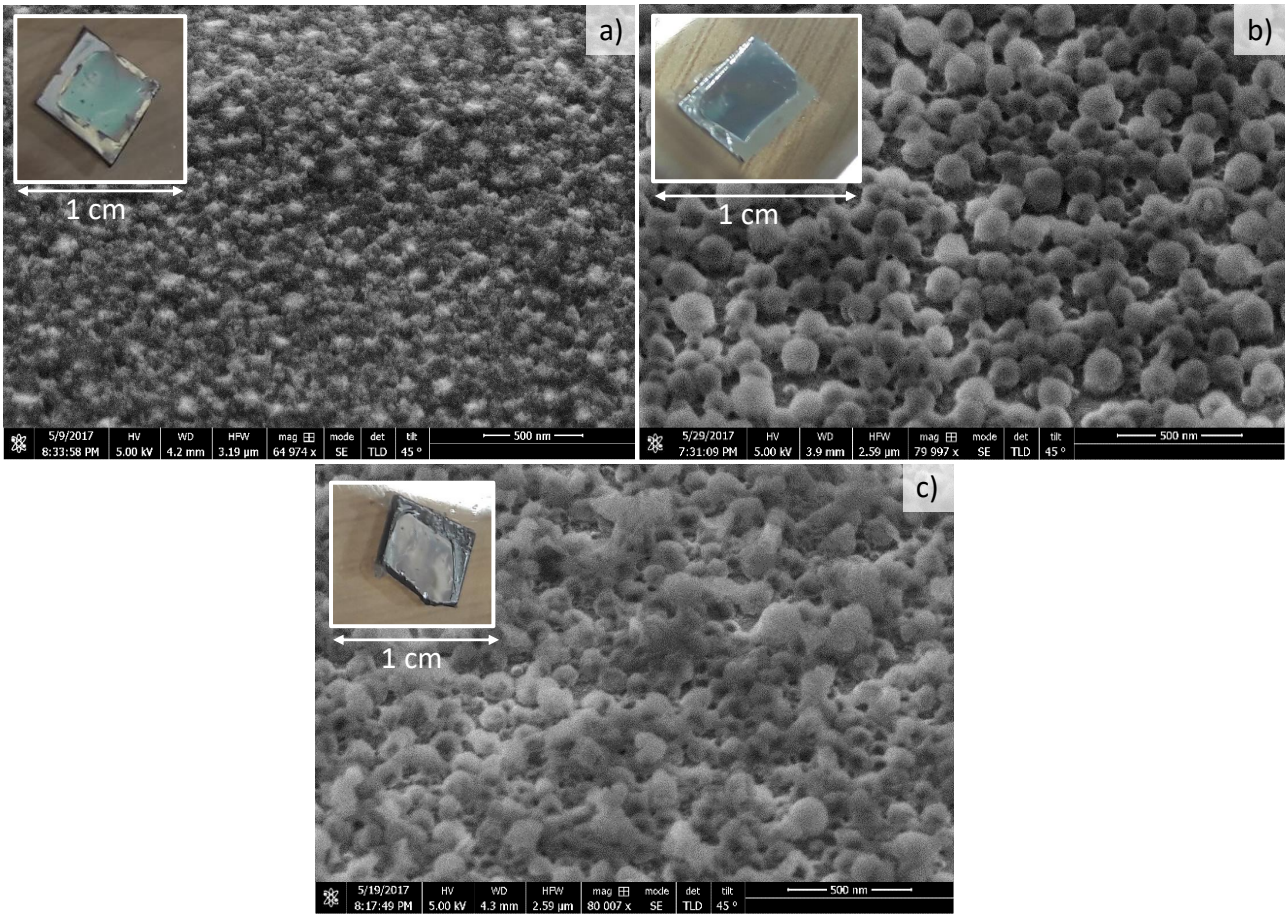

Figure 6.14: Si deposition on Si+Ga: (a) Room temperature, (b) 45°C, (c) 65°C. In the insets: color of the sample. SEM pictures taken with samples tilted at 45°.

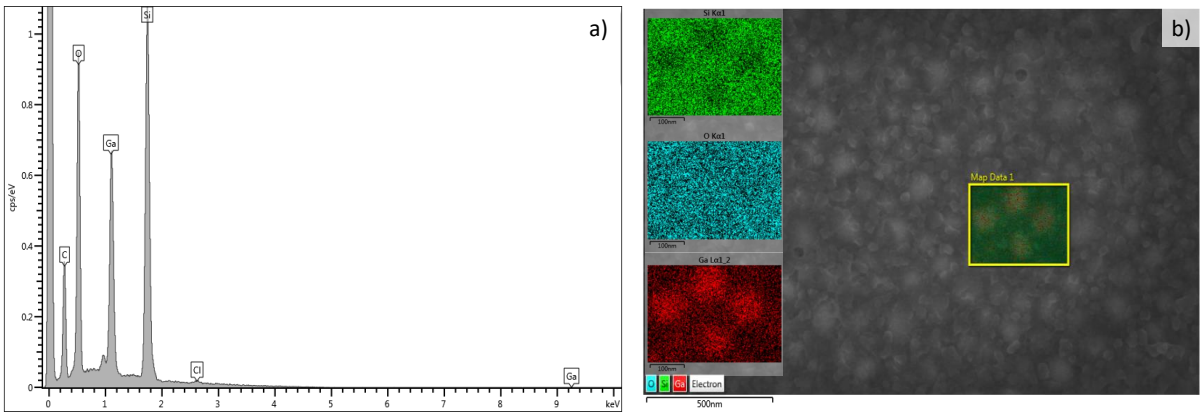

Figure 6.15: EDX analysis for electrodeposition on Si+Ga substrate at RT: (a) spectrum, (b) layered map and in the insets maps divided by element.

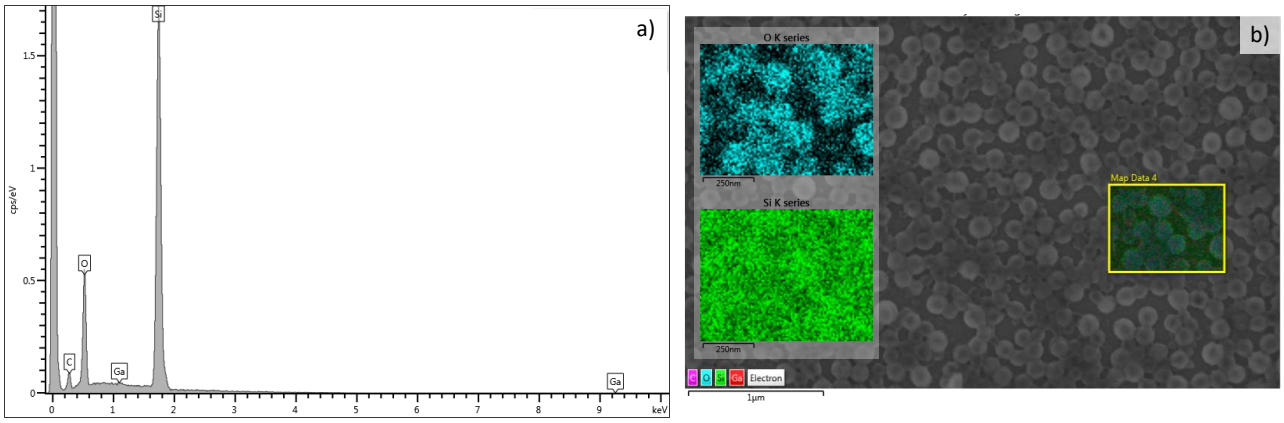

Figure 6.16: EDX analysis for electrodeposition on Si+Ga substrate at 45°C: (a) spectrum, (b) layered map and in the insets maps divided by element.

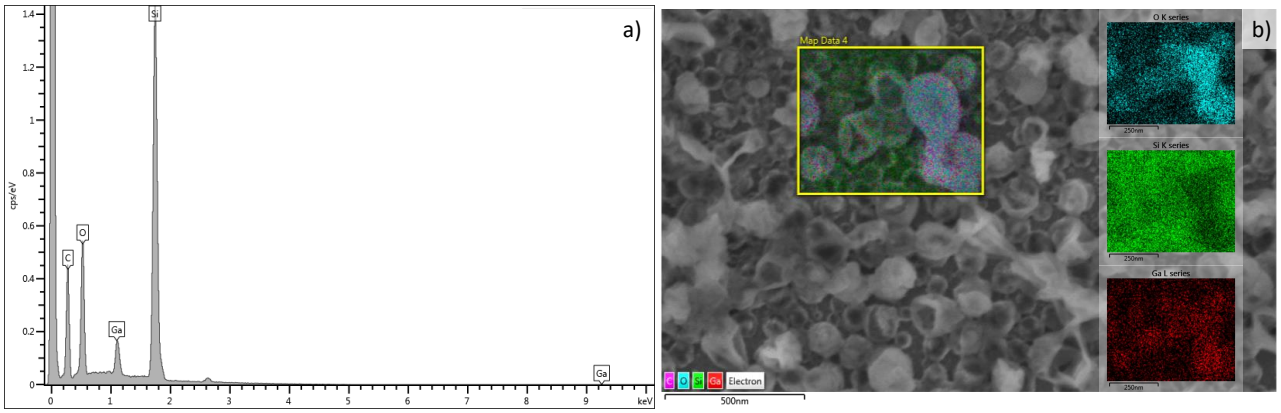

Figure 6.17: EDX analysis for electrodeposition on Si+Ga substrate at 65°C: (a) spectrum, (b) layered map and in the insets maps divided by element.

In fig. 6.14 are reported the SEM pictures of the depositions for RT, 45°C and 65°C with the aspect of the corresponding samples. At room temperature the deposition is completely covering the Ga droplets, they are still slightly visible from the SEM picture, but this is much more evident looking at the EDX analysis (fig. 6.15). For 45°C and 65°C the deposition is made of structures with rounded shape, the first hypothesis was that this shape was due to the Ga droplets, but looking at the EDX for the case of 45°C (fig. 6.16) no traces of Ga are detected, unlike the case of 65°C (fig. 6.17). This raises doubts about the role of Ga on the growth.

Actual photographs of the samples have been reported because it is interesting to note that they show different colors. The colors can be related to the thickness or to the nanostructuring of the deposition [73][74][75].

It is known that dielectrics with size features around that of visible wavelenghts are strong light scatterers for particular colors. This would provide a colored appearance to the nanostructures that depends on their size [74]. An example is shown in fig. 6.18.

Another possibility that offers colored appearance arises from multiple reflections and inter-

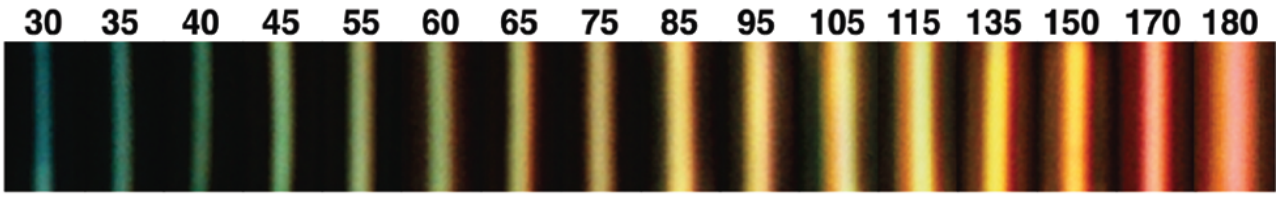

Figure 6.18: Size-dependent multicolor light scattering of individual Si nanowires. The numbers represents the diameters of the nanowire in nm [74].

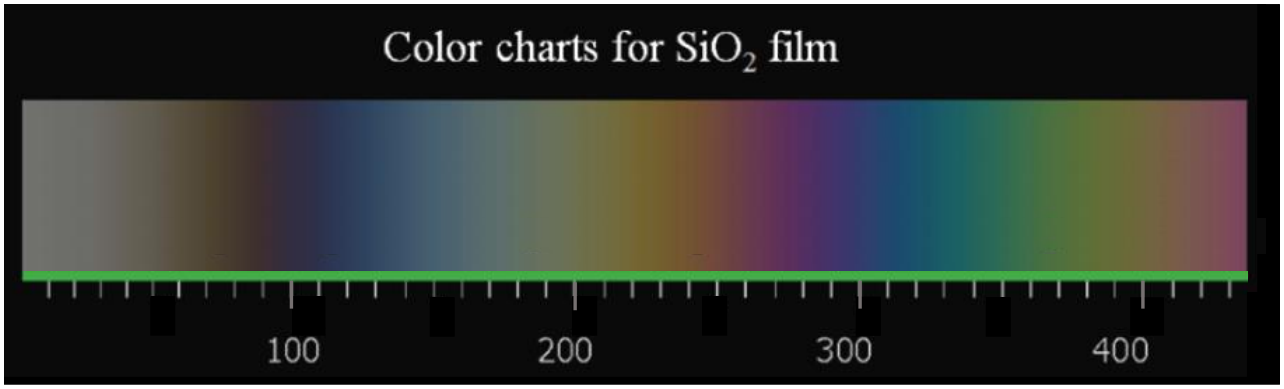

Figure 6.19: Color charts for SiO_2 films. The numbers represents the SiO_2 thickness in nm. Adapted from [75].

ference at thin SiO_X layers on Si (which has a larger refractive index) [75]. The dependence of color from thickness is shown in fig. 6.19.

By comparing these charts with the colors of the samples in fig. 6.14 it seems that the main contribution is coming from the diameter of the nanostructures, which in this case is therefore lower than 80 nm.

In the case of a Si substrate the EDX analysis is less useful since it is difficult to distinguish

Temperature	Peak position
RT	102.75 ± 0.15 eV
45°C	103.08 ± 0.15 eV
65°C	103.80 ± 0.15 eV

Table 6.6: XPS peak position for deposition on Si+Ga substrate at room temperature, 45°C and 65°C.

between the contributes coming from the deposition or from the substrate, what is more evident is the difference in the amount of oxygen: the deposition seems more oxidized than the substrate. In this case it is therefore even more important to analyze the sample with the XPS. The characteristics of the measurements are the same as described for the Al substrate, the experimental peaks positions for the different temperatures are shown in table 6.6.

The peaks are plotted in fig. 6.20 and can be compared again with the theoretical values of

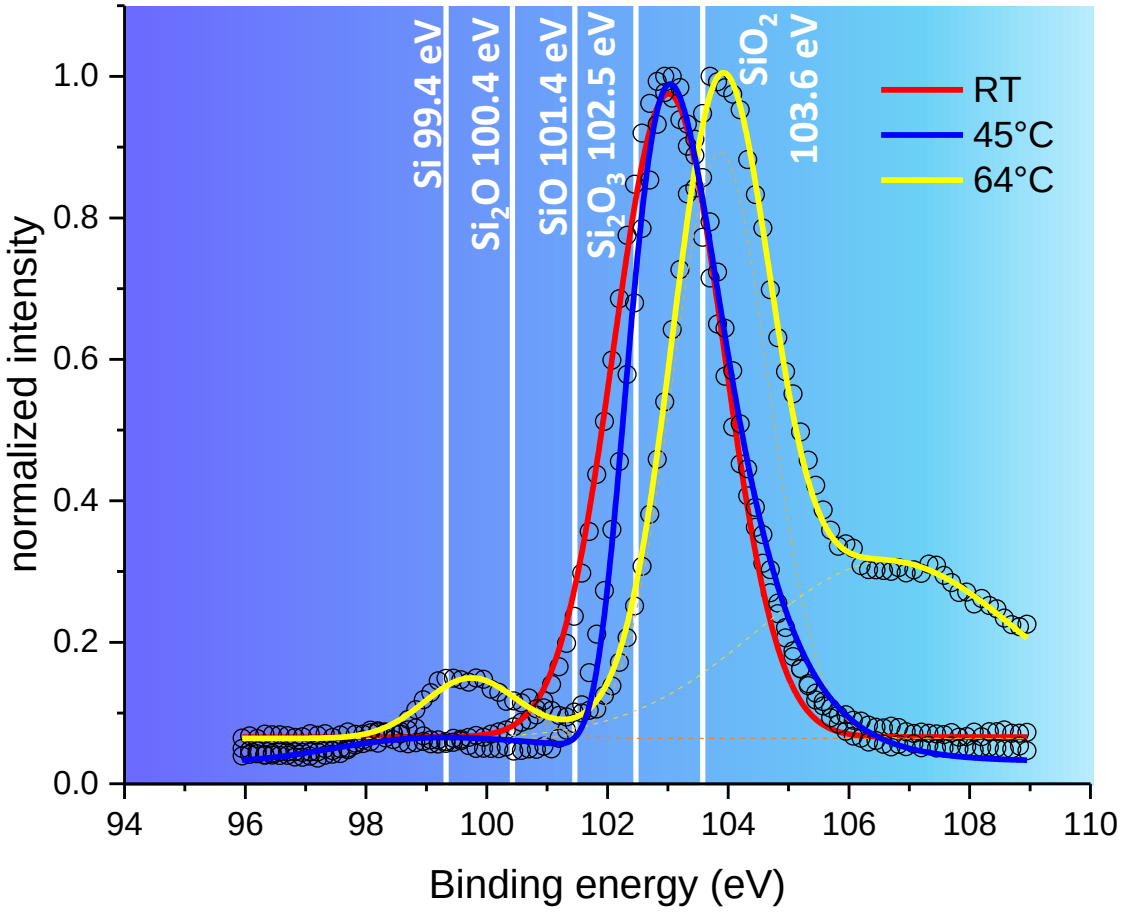

Figure 6.20: XPS peaks for deposition on Si+Ga substrate at room temperature (red), 45°C (blue) and 65°C (yellow). The white lines represent the energies of the different oxidation levels of Si. The intensity has been normalized since it is related to optimization processes performed independently for every sample.

the oxidation states in table 6.3. Similarly to the case of Al an increase of the oxidation level

with the temperature is observed, although less evident. In particular the deposition at room temperature is much more oxidized than in the case of the Al substrate.
As compared to the Al case, a second peak at 100 eV is observed and it is most likely due to the substrate. This is confirmed with a reference measurement performed on a sample with just Si and Ga. Since the XPS depth is of few nanometers this signal is probably coming from some empty spaces between the structures. The origin of the "shoulder" visible at higher energies for the peak at 65°C is still under investigation.

6.4 The influence of voltage on the deposition

For almost all the samples the deposition has been performed at different voltages[3] for each temperature, keeping always in mind the voltammograms in fig. 6.8. First it has been analyzed how the deposition changes by increasing the voltage for a certain temperature. Second, samples at different temperature and voltages have been characterized through XPS in order to assess the effect of the voltage on the oxidation state of the deposition.
In picture 6.21 depositions at room temperature on SS+Ga substrate for different voltages are

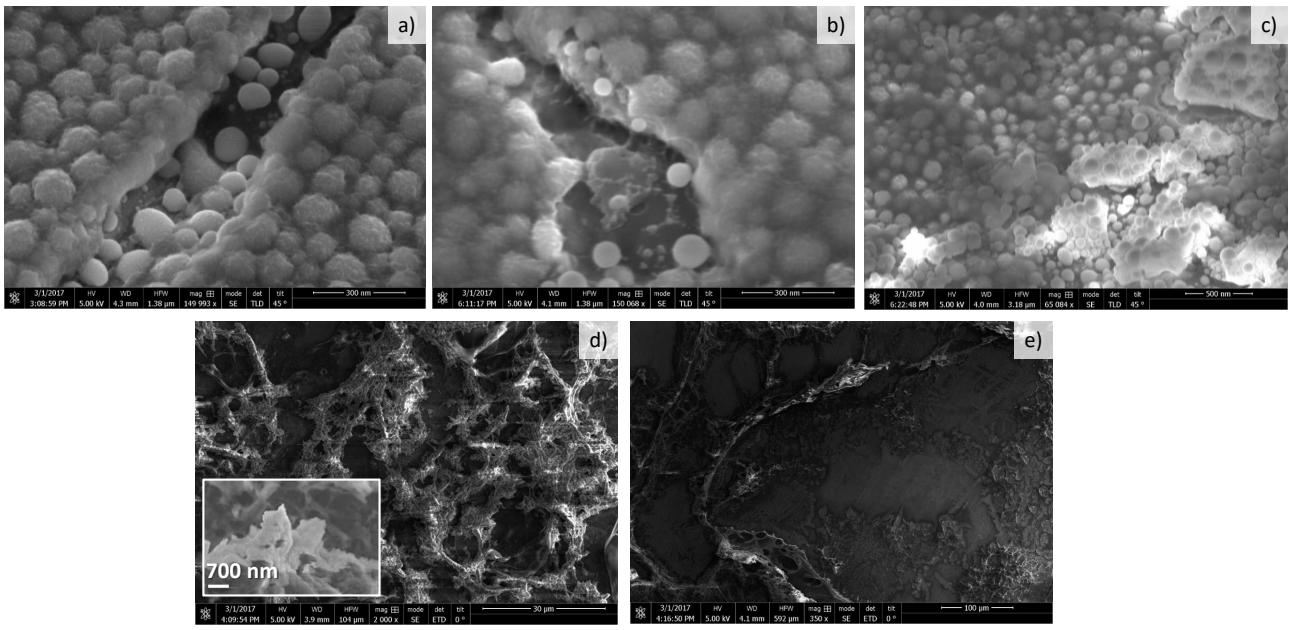

Figure 6.21: Depositions at different applied voltages os SS+Ga substrate at room temperature: (a) -1.6V, (b) -2.15V, (c) -2.8V, (d) -3.15V, (e) -6V. Pictures (a), (b) and (c) taken with samples tilted at 45°.

shown. The CV of reference is the one at room temperature in fig. 6.8 (blue curve).
Voltages from -1.6V to -6V were used, considering that at $\sim$ -3V the current is also due to reactions related to the other elements of the solution (black curve in fig. 6.8). For example it

[3]The voltage is always the potential difference WE vs PtQRE, where PtQRE stand for Pt quasi-reference.

is possible that at that voltage, which will be called *limit voltage* (V_L), the electrolyte starts to break. From the SEM pictures is evident a progressive change in the homogeneity of the deposition with the increase of the voltage: at -1.6V the Ga droplets are consistently covered by a layer of Si (the identity of the grown material is again confirmed by EDX analysis), increasing the voltage this layer becomes thicker until it starts to break (fig. 6.21c). This happens when the voltage is close to the values of V_L, suggesting that the cracking of the deposition is an effect of what is happening to solvent and supporting electrolyte. Indeed the successive two pictures for deposits at -3.5V and -6V show a completely disordered and irregular deposition, the pictures have been taken with a much lower magnification compared to the others in order to point out more clearly the non homogeneous distribution of the deposited material for those voltages.
The same behavior has been noticed repeating this kind of test on the others substrates.

To check if the applied voltage has an influence on the oxidation state of the deposition, several samples from different substrates and temperatures has been analyzed with XPS. The single spectra are reported in the appendix, the results are here summarized in fig. 6.22 in which are also represented the positions of the theoretical binding energies for Si oxidation states. The precise peak positions are listed in tables 6.7 and 6.8.

It is possible to see a trend in the oxidation state of the depositions: every color represents the XPS peaks for a certain substrate and a certain temperature and there's a general trend of reduction of the oxidation with the increasing of the voltage.

Al+Ga substrate				*SS+Ga substrate*	
45°C		**65°C**		**45°C**	
-3.6V	**-4.6V**	**-3.3V**	**-3.6V**	**-2.15V**	**-3.5V**
103.26 ± 0.15 eV	101.52 eV ± 0.15 eV	103.80 ± 0.15 eV	103.66 ± 0.15 eV 102.82 ± 0.15 eV	104.26 ± 0.15 eV	104.05 ± 0.15 eV

Table 6.7: XPS peak positions depending on voltage and temperature for Al+Ga and SS+Ga substrates.

Si+Ga substrate				
RT		**65°C**		
-2.5V	**-3.5V**	**-2V**	**-2.5V**	**-3V**
102.80 ± 0.15 eV	102.74 ± 0.15 eV	104.1 ± 0.2 eV	103.80 ± 0.15 eV	103.77± 0.15 eV

Table 6.8: XPS peak positions depending on voltage and temperature for Si+Ga substrate.

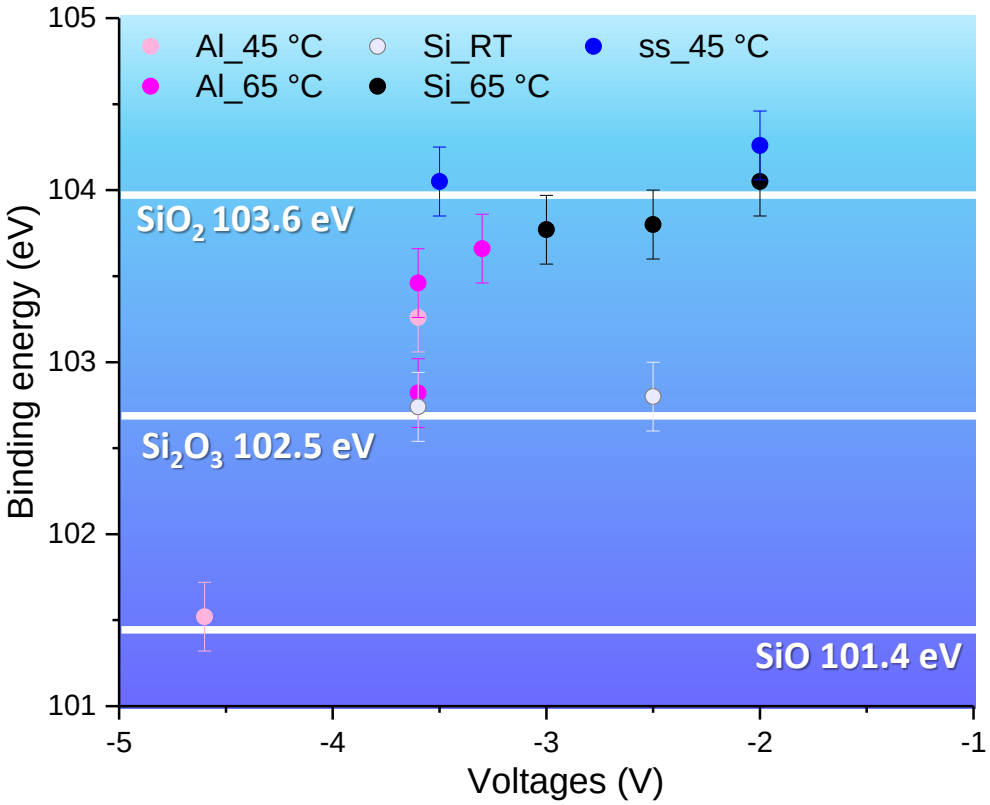

Figure 6.22: Trend of binding energy in relation with a change in the voltage employed for the deposition. Every point represents a XPS peak position at a certain voltage, divided by substrate and temperature. The white lines represent the energies of the different oxidation levels of Si.

6.5 Electrodeposition on substrates without Ga

In order to have reference measurements a test has been performed at 65°C on Al and Si substrates *without* evaporated Ga on the top. It has been chosen to do it at 65°C because at that temperature Ga is expected to be liquid, so it is possible to check if its presence actually affects the deposition or not. The parameters of the deposition are reported in table 6.9.

Substrate	Voltage (WEvsPtQRE)	Deposited charge
Si	-2.5 V	0.13C
Al	-3.3 V	0.13C

Table 6.9: Parameters for electrodeposition on Si and Al substrate at 65°C.

In fig. 6.23 and 6.24 are presented the SEM pictures of the two depositions compared with the respective depositions on substrates with Ga (same temperature, voltage and deposited charge). EDX analysis confirmed that the deposited material is Si. It is clear that the amount

of deposited material is larger in the substrates with Ga. Round shaped nanostructures are visible either in the substrate with Ga and in those without, this rises again doubts about the fact that the rounded shape (noticed also in the depositions shown in the previous sections) is related to the shape of the Ga droplets.

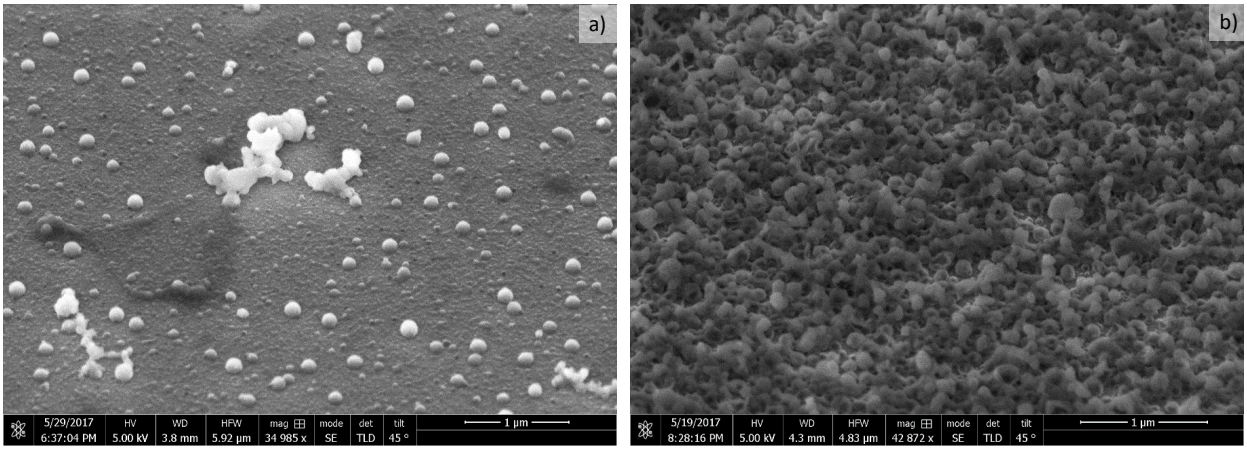

Figure 6.23: Deposition at 65°C and -2.5V on Si (a) and Si+Ga (b) substrate. Pictures taken with samples tilted at 45°.

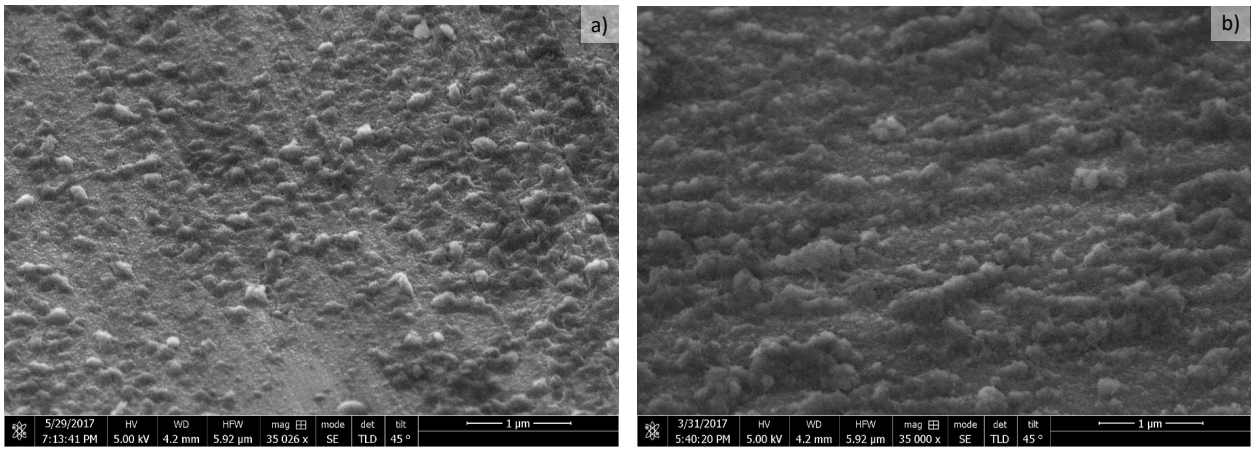

Figure 6.24: Deposition at 65°C and -3.3V on Al (a) and Al+Ga (b) substrate. Pictures taken with samples tilted at 45°.

Moreover if the XPS spectra of the depositions on substrates with and without Ga (fig. 6.25) are compared it is possible to see that the oxidation state is basically the same, the deposited material is even slightly less oxidized in the case without Ga. It therefore seems that the presence of Ga on the surface is not really affecting the deposition, at least in terms of quality.
Nevertheless, it is also possible that the structures visible in the samples without Ga are not due to the deposition, but to precipitation of SiO_2 from the solution, since, looking at the reaction in eq. 4.2, it can be created if the solution enters in contact with air (i.e. if the cell is

not properly sealed). Further experiments are needed to confirm or deny this hypothesis.

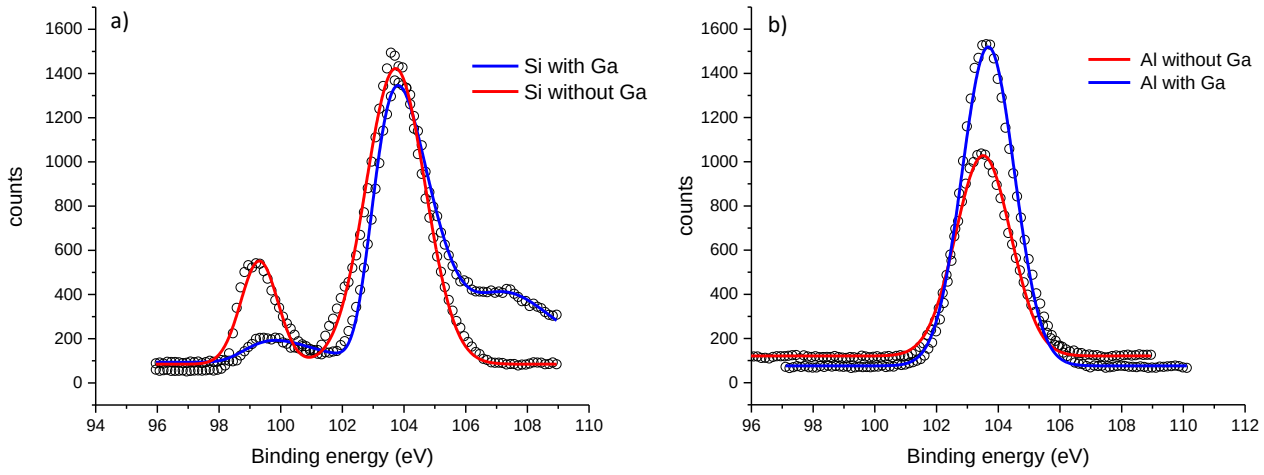

Figure 6.25: XPS peaks for depositions with and without Ga on (a) Si substrate and (b) Al substrate.

CHAPTER 7

Conclusions

In this work the electrochemical deposition of Si at low temperatures using Ga as catalyst has been investigated.
Ga has been deposited through thermal evaporation on different substrates. For most of the samples the result has been a distribution of droplets due to the fact that, during the evaporation, Ga gathers thanks to surface diffusion and Ostwald ripening. The diameter of the droplets can be tuned by changing the nominal thickness of the deposition.
Silicon has been successfully deposited on different substrates, in particular on Al+Ga, Si+Ga and stainless steel+Ga, at different temperatures up to 65°C and at different voltages. Moreover an electrochemical cell has been designed and custom-build, and has been proven successful for the purpose of this work.
It has been therefore possible to characterize the effect of the different parameters on the deposition and a correlation between temperature/voltage and some characteristics of the deposition, such as oxidation state, homogeneity and amount of grown material has been noticed.
As a general trend it has been found that increasing the temperature brings to a thicker deposition, despite the amount of current registered at the working electrode is the same. This suggests that the higher the temperature is the larger percentage of the current is actually due to the reduction of the Si ions. Moreover through XPS analysis it has been possible to assess that the oxidation of the deposition increases with the temperature and this could be an indication of the level of porosity of the material. The same set of measurements revealed also that in general the deposition presents an oxidation state very similar to that of SiO_2.
Performing experiments at different voltages has also allowed some considerations. First of all, if substrate and temperature are fixed, it is possible to see a progressive change in the morphology of the deposition related to the driving bias. More specifically, at low voltages (in absolute value) the deposition appears homogeneous, but it starts to "crack" as soon as the voltage approaches the value of V_L, which corresponds to the potential at which other reactions occur (i.e. related to the solvent or the supporting electrolyte). All the experiments performed

at voltages higher than V_L show a very irregular and disordered deposition.
Second, XPS measurements stressed the presence of a relation between voltage and oxidation state. Fixing temperature and potential, it is possible to notice that the highest the voltage the lowest is the oxidation. The same trend is observed for different substrates and temperatures. A possible explanation for this behavior can be related to the speed of the deposition. Indeed the higher the voltage the fastest is the deposition for the same amount of charge (i.e. Si atoms). It is possible that if the deposition is faster, the Si atoms are packing more, leaving therefore less free "space" for oxygen to be trapped afterwards. However this behavior is still under investigation.
What follows from these last considerations is that for obtaining an homogeneous deposition it is advisable to employ a low voltage (between the range of potentials suitable for the experiment) and not to overcome V_L. At the same time, however, the grown material appears less oxidized for higher voltages, and this brings to a contradiction about the approach to follow. A possible solution could be provided by Ga, indeed, if it works as catalyst driving the growth of crystalline Si, than the quality of the material should be good also for low voltages.
At the moment there are still a lot of open questions, especially the oxidation process has to be further investigated in order to understand if it is happening after the experiment or if it is due to the presence of traces of oxygen in the solution. Up to now it has not been possible to characterize directly the level of porosity of the material and how amorphous/crystalline it is. Another thing which is not clear is the actual effect of Ga in the process, but it seems that under current conditions Ga is not clearly playing a role. This could be related to the presence of Ga native oxide on the surface of the droplets, since there are evidences that, in ec-LLS processes, changes in the surface properties of the liquid metal may be important [9]. It is also possible that the droplets are too small for performing the experiment at the current conditions, for future experiments one should try droplets with a bigger diameter and lowering it only once established the proper conditions for obtaining crystalline Si.
These are therefore the main conditions which may be useful to change, it could be also interesting to see if there is an improvement by applying a voltage much lower than those employed in this work. Moreover new conditions could be taken into account, for example the application of an external pressure, as done in other works related to this process [12].
In conclusion there is still a lot of interesting work to do in order to exploit the ec-LLS process in the case presented in this thesis, now the system has been better understood and is more clear how it reacts to different parameters, therefore the hope is that will be soon possible to actually apply this powerful method for growing silicon nanostructures.

CHAPTER 8

Appendix

8.1 Standard operating procedure (SOP)

Description of the experiment: Electrochemical synthesis of Silicon nanostructures

Equipment used: glovebox, fume hood, glass vials, weighing balance, nitrogen gas, plastic syringes, metallic needles, electrochemical cell.

Nature of hazards:

1. Hazardous substances (see table 8.1).
2. Sharps - danger of accidental puncture of skin with syringe needle.
3. Inert gases (N_2) - danger of asphyxiation.

Solutions: the solutions used are Propylene Carbonate (PC) + Tetraethylammonium chloride (TEAC) and Propylene Carbonate (PC) + Tetraethylammonium chloride (TEAC) + $SiCl_4$. $SiCl_4$ concentration can't be more than 0.7 M, otherwise the solution reaches supersaturation.

Reactions: $SiCl_4$ reacts with water in an exothermic vigorous reaction releasing a toxic gas (HCl):

$$SiCl_{4(l)} + 2H_2O_{(l)} \rightarrow SiO_{2(s)} + 4HCl_{(g)} \tag{8.1}$$

The electrochemical reactions involved in this electrodeposition experiment are:
Reduction reaction: $Si^{4+} + 4e^- \rightarrow Si$

Oxidation reaction: $2Cl^- \rightarrow Cl_2 + 2e^-$

Precautions: *Fume hood and glovebox*: ensure that the fume hood is working whenever handling chemicals in it. Contact proper personnel if it is not working.
$SiCl_4$ or any solution containing this compound must be always handled under a water-free environment (i.e. nitrogen or argon glove box). At high temperatures (> 200°C) a backpressure is needed to overcome the volatility of $SiCl_4$ (2.76 MPa).
The chemical reactions involved in an electrodeposition experiment occur in an electrochemical cell that must be filled and sealed in a glovebox.
Protective gloves (nitrile rubber, 0.11 mm, 480 min), lab coat and goggles must be worn at all times when in the lab. The containers with the solution and the chemicals involved in its preparation must be used and stored in a glovebox. If it's necessary to take the solution out of the glovebox the container must be sealed.

Procedure:

1. Prepare the solutions inside the glovebox. $SiCl_4$ can poison the catalyst that removes oxygen from the glovebox, so turn off the circulation of the glovebox and start the purging process when using $SiCl_4$ in the glovebox. After finishing let the glovebox purge for some hours and then turn on the circulation again. For purging procedure see the glovebox SOP.

2. In the hood, glue the substrate to a microscope slide covered with Al foil.

3. Bring the cell and the sample inside the glovebox.

4. In the glovebox, mount the sample in the cell, fill the cell with the solution and seal the cell.

5. Transfer the cell from the glovebox to the hood by using a secondary container, to prevent any contamination in case of accident.

6. In the hood, connect properly working, counter and reference electrode to the cell and to the potentiostat and perform the experiment.

7. Once finished, transfer the cell from the hood to the glovebox together with tweezers, 2 beakers and enough parafilm to cover them afterwards.

8. In the glovebox open the cell, take off the sample and clean it properly with PC (use one of the beaker to collect PC and solution from the cleaning process), then store the sample in the other beaker filled with PC and close the beaker with parafilm.

9. If another electrochemical test has to be performed, repeat from point 4.
10. Every time a sample is removed from the cell, then transfer the beaker with the sample to the hood, clean the sample with acetone, dry it with N_2 and store it.
11. Once the last test is finished, clean and store the sample as in point 8, then empty the cell in the beaker with $SiCl_4$ containing waste and clean the cell with PC. Close the beaker with parafilm.
12. Transfer the empty cell, the beaker with the last sample and the beaker with $SiCl_4$ containing waste to the hood by using a secondary container.
13. Clean again the cell with acetone and deionized water, clean and store the sample as in point 10, dispose of the $SiCl_4$ containing waste. Proper $SiCl_4$ waste disposal is explained below.

$SiCl_4$ waste disposal:

1. In the hood, Prepare water in a cooled vessel (temperature should be no more than room temperature) with volume 5-10 times that of the solution to be neutralised and start stirring.
2. Slowly pour the $SiCl_4$ containing solution and let the HCl gas evolve and flow in the hood.
3. Let stir for around 20 minutes, then the solution in the vessel is neutralised. This can be poured into the waste bin for organic acids (red can).

	silicon tetrachloride CAS No. 10026-04-7	**propylene carbonate** CAS No. 108-32-7	**TEAC** CAS No. 56-34-8
Hazard statements	H319 Causes serious eye irritation H335 May cause respiratory irritation H315 Causes skin irritation	H319 Causes serious eye irritation	H302 Harmful if swallowed H315 Causes skin irritation H318 Causes serious eye damage Toxic to aquatic organism
Storage and transportation	Store in cool, dry, protected area. Dispose of this material and its container at hazardous or special waste collection point. Keep out of reach of children. Keep container tightly closed. Keep container dry.	Store in cool, dry, protected area. Dispose of this material and its container at hazardous or special waste collection point. Keep out of reach of children. Handle and open container with care	Store in cool, dry, protected area. Dispose of this material and its container at hazardous or special waste collection point. Keep out of reach of children. Keep away from food, drink and animal feeding stuffs
Fire/Explosion Hazard	Vapours/gas heavier than air. Toxic smoke/fumes in a fire. Attacks metals to liberate hydrogen. Reacts VIOLENTLY with water. Dispose of this material and its container at hazardous or special waste collection point	Vapours/gas heavier than air. Toxic smoke/fumes in a fire. Dispose of this material and its container at hazardous or special waste collection point	Toxic smoke/fumes in a fire. Dispose of this material and its container at hazardous or special waste collection point

Table 8.1: Nature of hazards for the chemicals used in the experiment

8.2 List of samples

Sample	Substrate	Temperature	Voltage (WEvsPtQRE)	Deposited charge	Analysis
ssRT-1	ss+Ga	RT	-1.6 V	0.008C	SEM, EDX, XPS
ssRT-2	ss+Ga	RT	-2.15 V	0.013C	SEM, EDX, XPS
ssRT-3	ss+Ga	RT	-2.8 V	0.010C	SEM, EDX, XPS
ssRT-4	ss+Ga	RT	-3.5 V	0.25C	SEM, EDX, XPS
ssRT-5	ss+Ga	RT	-6 V	1.100C	SEM, EDX, XPS
ss45-1	ss+Ga	45°C	-2 V	0.030C	SEM, EDX
ss45-2	ss+Ga	45°C	-2.8 V	0.034C	SEM, EDX
ss45-3	ss+Ga	45°C	-3.5 V	2.057C	SEM, EDX
ss45-4	ss+Ga	45°C	-4 V	2.005C	SEM, EDX
ss45-5	ss+Ga	45°C	-2.8 V	0.400C	SEM, EDX
ss45-6	ss+Ga	45°C	-4.2 V	3.485C	SEM, EDX
ss45-7	ss+Ga	45°C	-2 V	0.029C	SEM, EDX, XPS
ss45-8	ss+Ga	45°C	-3.5 V	1.383C	SEM, EDX, XPS
CuRT-1	Cu+Ga	RT	-3.8 V	1.128C	SEM, EDX
CuRT-2	Cu+Ga	RT	-2.28 V	0.009C	SEM, EDX
MoRT-1	Mo+Ga	RT	-3.6 V	0.245C	SEM, EDX
MoRT-2	Mo+Ga	RT	-3 V	0.334C	SEM, EDX
Al45-1	Al+Ga	45°C	-3.6 V	0.006C	SEM, EDX, XPS
Al45-2	Al+Ga	45°C	-4.6 V	0.564C	SEM, EDX, XPS
Al45-3	Al+Ga	45°C	-3.6 V	0.060C	SEM, EDX, XPS
Al45-4	Al+Ga	45°C	-4.6 V	1.160C	SEM, EDX, XPS
Al65-1	Al+Ga	65°C	-3.6 V	0.300C	SEM, EDX, XPS
Al65-2	Al+Ga	65°C	-3.3 V	0.030C	SEM, EDX, XPS
Al65-3	Al+Ga	65°C	-3.6 V	0.030C	SEM, EDX, XPS
Al65-4	Al+Ga	65°C	-3 V	0.030C	SEM, EDX, XPS
Al65-5	Al+Ga	65°C	-3.6 V	0.130C	SEM, EDX, XPS
Al65-6	Al+Ga	65°C	-3.3 V	0.130C	SEM, EDX, XPS
Al65-7	Al+Ga	65°C	-3.6 V	0.340C	SEM, EDX, XPS
Al80-1	Al+Ga	80°C	-2.5 V	0.130C	SEM
Al80-2	Al+Ga	80°C	-3 V	0.130C	SEM
Al80-3	Al+Ga	80°C	-3.5 V	0.130C	SEM
Al80-4	Al+Ga	80°C	-3.5 V	0.130C	SEM
Al80-6	Al+Ga	80°C	-3 V	0.130C	SEM
Al80-7	Al+Ga	80°C	-3.5 V	0.340C	SEM
AlRT-1	Al+Ga	RT	-2.5 V	0.030C	SEM, EDX, XPS
Al45-5	Al+Ga	45°C	-3.6 V	0.130C	SEM, EDX, XPS
SiRT-1	Si+Ga	RT	-2.5 V	0.130C	SEM, EDX, XPS
SiRT-2	Si+Ga	RT	-3.6 V	0.130C	SEM, EDX, XPS
Si65-1	Si+Ga	65°C	-2 V	0.130C	SEM, EDX, XPS
Si65-2	Si+Ga	65°C	-2.5 V	0.130C	SEM, EDX, XPS
Si65-3	Si+Ga	65°C	-3 V	0.130C	SEM, EDX, XPS
Si80-1	Si+Ga	80°C	-2.5 V	0.130C	SEM
Si80-2	Si+Ga	80°C	-2.5 V	0.130C	SEM
Si45-1	Si+Ga	45°C	-2 V	0.130C	SEM, EDX
Si65-4	Si	65°C	-2.5 V	0.130C	SEM, EDX
Al65-8	Al	65°C	-3.3 V	0.130C	SEM, EDX
Si65-5	Si	65°C	-2.5 V	0.130C	SEM, EDX, XPS
Al65-9	Al	65°C	-3.3 V	0.130C	SEM, EDX, XPS
Si45-2	Si+Ga	45°C	-2 V	0.130C	SEM, EDX, XPS

Table 8.2: List of all the chronoamperometry performed at different conditions. Chronological order.

8.3 Experimental results: XPS measurements for different voltages

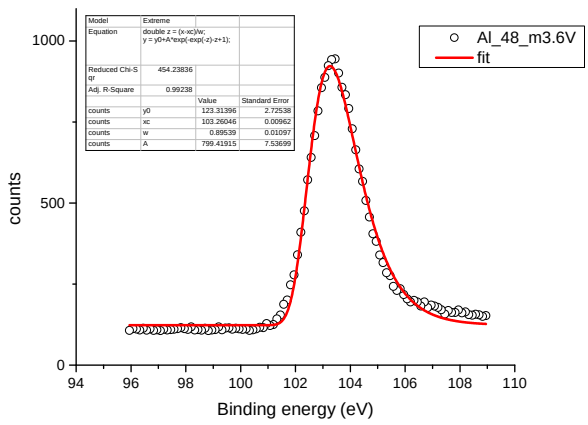

Figure 8.1: **sample Al45-1** - XPS spectrum

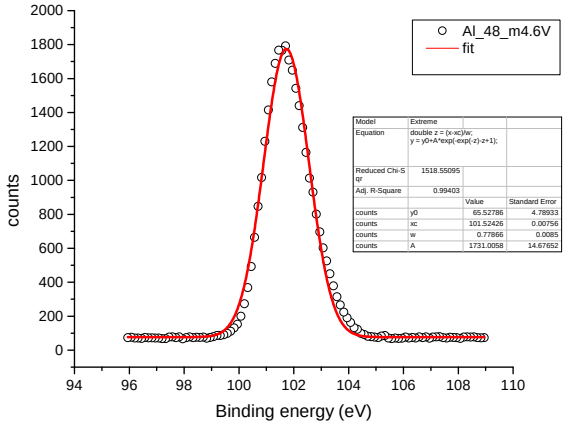

Figure 8.2: **sample Al45-2** - XPS spextrum

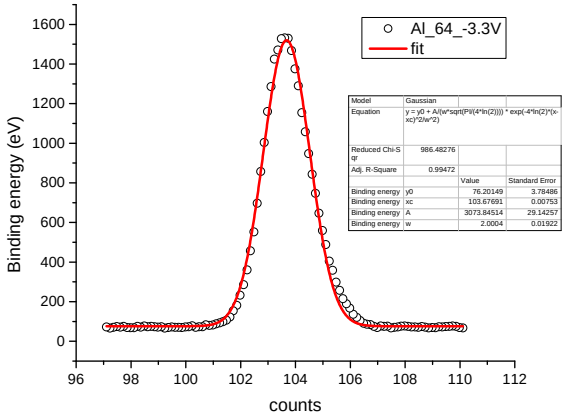

Figure 8.3: **sample Al65-2** - XPS spectrum

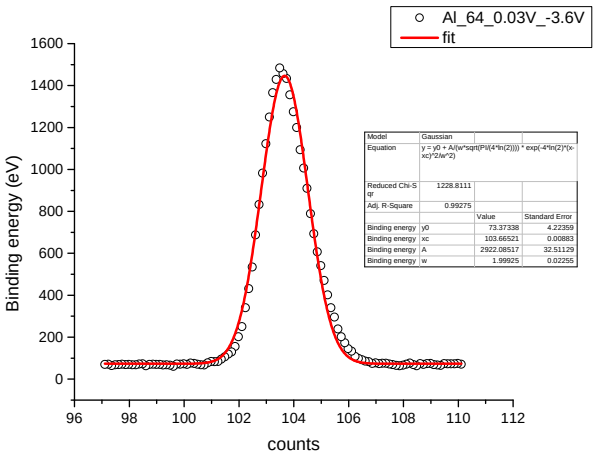

Figure 8.4: **sample Al65-3** - XPS spextrum

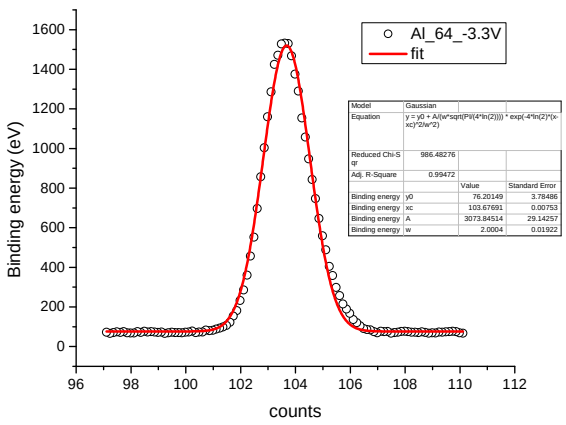

Figure 8.5: **sample Al65-7** - XPS spectrum

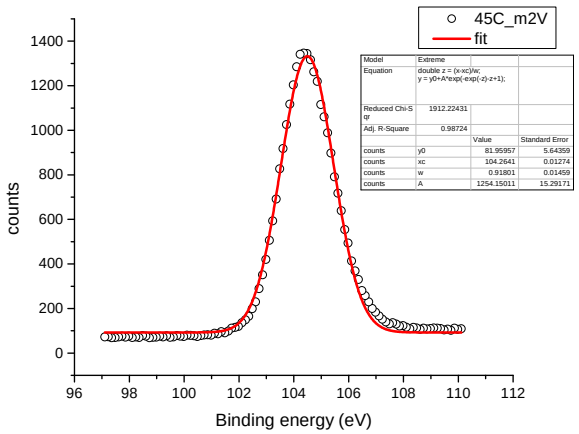

Figure 8.6: **sample ss45-7** - XPS spextrum

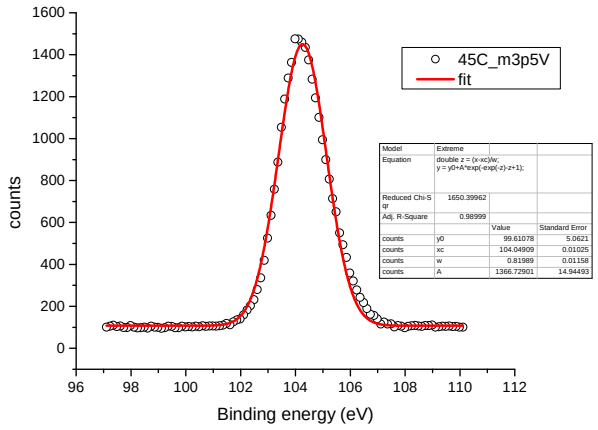

Figure 8.7: **sample ss45-8** - XPS spectrum

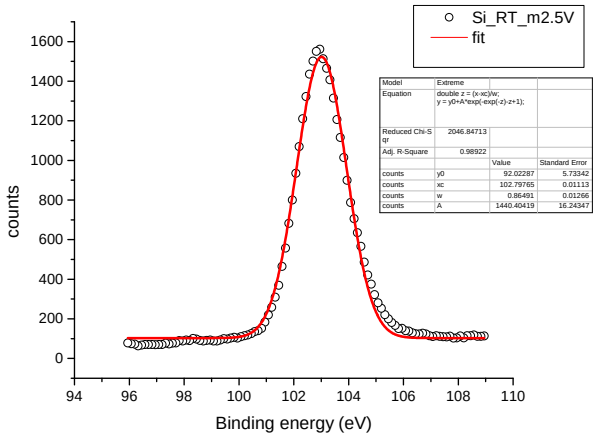

Figure 8.8: **sample SiRT-1** - XPS spextrum

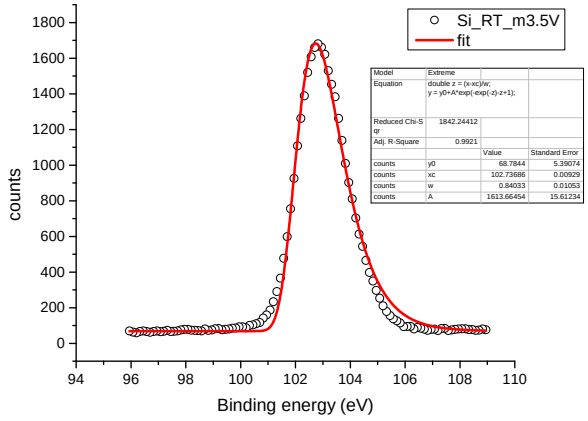

Figure 8.9: **sample SiRT-2** - XPS spectrum

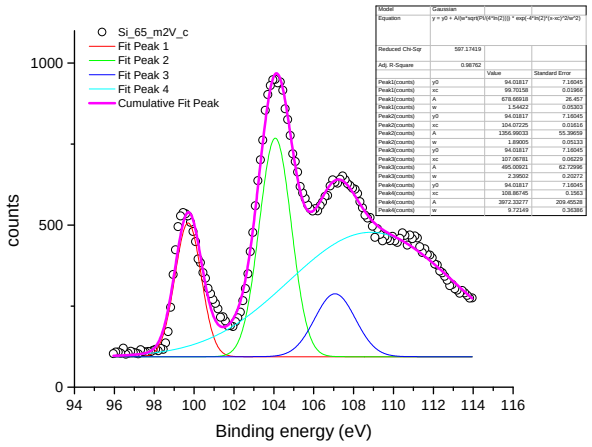

Figure 8.10: **sample Si65-1** - XPS spextrum

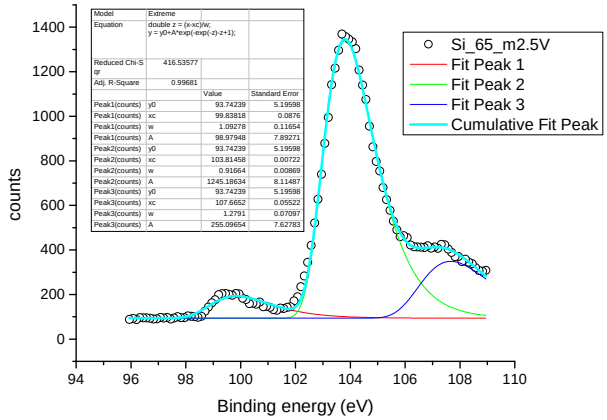

Figure 8.11: **sample Si65-2** - XPS spectrum

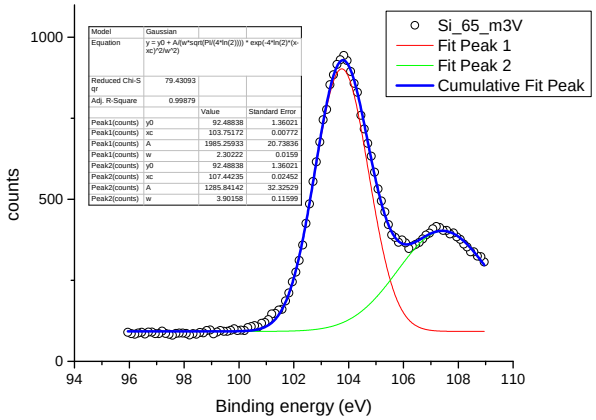

Figure 8.12: **sample Si65-3** - XPS spextrum

Bibliography

[1] Jianhua Zhao, Aihua Wang, Martin A. Green, and Francesca Ferrazza. 19.8% efficient "honeycomb" textured multicrystalline and 24.4% monocrystalline silicon solar cells. *Applied Physics Letters*, 73(14):1991–1993, 1998.

[2] William Shockley and Hans J. Queisser. Detailed balance limit of efficiency of p-n junction solar cells. *Journal of Applied Physics*, 32(3):510–519, 1961.

[3] Albert Polman and Harry A. Atwater. Photonic design principles for ultrahigh-efficiency photovoltaics. *Nature Materials*, 11(3):174–177, 2012.

[4] Mark L. Brongersma, Yi Cui, and Shanhui Fan. Light management for photovoltaics using high-index nanostructures. *Nature Materials*, 13(5):451–460, 2014.

[5] Erik Garnett and Peidong Yang. Light trapping in silicon nanowire solar cells. *Nano Letters*, 10(3):1082–1087, 2010.

[6] Francesco Priolo, Tom Gregorkiewicz, Matteo Galli, and Thomas F. Krauss. Silicon nanostructures for photonics and photovoltaics. *Nature Nanotechnology*, 9(1):19–32, 2014.

[7] Gopalakrishna M. Rao. Electrowinning of silicon from K2SiF6-molten fluoride systems. *Journal of the Electrochemical Society:Electrochemical Science and Technology*, 127(9):1940–1944, 1980.

[8] Dennis Elwell and Robert S. Feigelson. Electrodeposition of solar silicon. *Solar Energy Materials*, 6(2):123 – 145, 1982.

[9] Eli Fahrenkrug and Stephen Maldonado. Electrochemical Liquid-Liquid-Solid (ec-LLS) Crystal Growth: A Low-Temperature Strategy for Covalent Semiconductor Crystal Growth. *Accounts of Chemical Research*, 48(7):1881–1890, 2015.

[10] Eli Fahrenkrug, Junsi Gu, Sunyeol Jeon, P. Alexander Veneman, Rachel S. Goldman, and Stephen Maldonado. Room-temperature epitaxial electrodeposition of single-crystalline germanium nanowires at the wafer scale from an aqueous solution. *Nano Letters*, 14(2):847–852, 2014.

[11] Eli Fahrenkrug, Junsi Gu, and Stephen Maldonado. Electrodeposition of crystalline gaas on liquid gallium electrodes in aqueous electrolytes. *Journal of the American Chemical Society*, 135(1):330–339, 1 2013.

[12] Junsi Gu, Eli Fahrenkrug, and Stephen Maldonado. Direct electrodeposition of crystalline silicon at low temperatures. *Journal of the American Chemical Society*, 135(5):1684–1687, 2013. PMID: 23347180.

[13] Mark L. Brongersma, Yi Cui, and Shanhui Fan. Light management for photovoltaics using high-index nanostructures. *Nature Materials*, 13(5):451–460, 2014.

[14] A. P. Alivisatos. Semiconductor clusters, nanocrystals, and quantum dots. *Science*, 271(5251):933–937, 1996.

[15] Y. Shirasaki, G. J. Supran, M. G. Bawendi, and V. Bulović. Emergence of colloidal quantum-dot light-emitting technologies. *Nature Photonics*, 7:13–23, January 2013.

[16] Dmitri V. Talapin, Jong-Soo Lee, Maksym V. Kovalenko, and Elena V. Shevchenko. Prospects of colloidal nanocrystals for electronic and optoelectronic applications. *Chemical Reviews*, 110(1):389–458, 2010. PMID: 19958036.

[17] K. Dohnalová, L. Ondič, K. Kůsová, I. Pelant, J. L. Rehspringer, and R.-R. Mafouana. White-emitting oxidized silicon nanocrystals: Discontinuity in spectral development with reducing size. *Journal of Applied Physics*, 107(5):053102, 2010.

[18] Kai-Yuan Cheng, Rebecca Anthony, Uwe R. Kortshagen, and Russell J. Holmes. High-efficiency silicon nanocrystal light-emitting devices. *Nano Letters*, 11(5):1952–1956, 2011. PMID: 21462935.

[19] A J Kenyon, P F Trwoga, M Federighi, and C W Pitt. Optical properties of pecvd erbium-doped silicon-rich silica: evidence for energy transfer between silicon microclusters and erbium ions. *Journal of Physics: Condensed Matter*, 6(21):L319, 1994.

[20] A Irrera, P Artoni, F Iacona, E F Pecora, G Franzò, M Galli, B Fazio, S Boninelli, and F Priolo. Quantum confinement and electroluminescence in ultrathin silicon nanowires fabricated by a maskless etching technique. *Nanotechnology*, 23(7):075204, 2012.

[21] L. T. Canham. Silicon quantum wire array fabrication by electrochemical and chemical dissolution of wafers. *Applied Physics Letters*, 57(10):1046–1048, 1990.

[22] O. Bisi, S. Ossicini and L. Pavesi. Porous silicon: a quantum sponge structure for silicon based optoelectronics. *Surface Science Reports*, 38(1):1–126, 2005.

[23] A.J Nozik. Quantum dot solar cells. *Physica E: Low-dimensional Systems and Nanostructures*, 14(1):115 – 120, 2002.

[24] Michael D. Kelzenberg, Daniel B. Turner-Evans, Brendan M. Kayes, Michael A. Filler, Morgan C. Putnam, Nathan S. Lewis, and Harry A. Atwater. Photovoltaic measurements in single-nanowire silicon solar cells. *Nano Letters*, 8(2):710–714, 2008. PMID: 18269257.

[25] M. D. Kelzenberg, S. W. Boettcher, J. A. Petykiewicz, D. B. Turner-Evans, M. C. Putnam, E. L. Warren, J. M. Spurgeon, R. M. Briggs, N. S. Lewis, and H. A. Atwater. Enhanced absorption and carrier collection in Si wire arrays for photovoltaic applications. *Nature Materials*, 9:239–244, March 2010.

[26] Thomas J. Kempa, Bozhi Tian, Dong Rip Kim, Jinsong Hu, Xiaolin Zheng, and Charles M. Lieber. Single and tandem axial p-i-n nanowire photovoltaic devices. *Nano Letters*, 8(10):3456–3460, 2008. PMID: 18763836.

[27] B. Tian, X. Zheng, T. J. Kempa, Y. Fang, N. Yu, G. Yu, J. Huang, and C. M. Lieber. Coaxial silicon nanowires as solar cells and nanoelectronic power sources. *Nature*, 449:885–889, October 2007.

[28] Y. Kanzawa, T. Kageyama, S. Takeoka, M. Fujii, S. Hayashi, and K. Yamamoto. Size-dependent near-infrared photoluminescence spectra of si nanocrystals embedded in sio2 matrices. *Solid State Communications*, 102(7):533 – 537, 1997.

[29] M. Zacharias, J. Heitmann, R. Scholz, U. Kahler, M. Schmidt, and J. Bläsing. Size-controlled highly luminescent silicon nanocrystals: A sio/sio2 superlattice approach. *Applied Physics Letters*, 80(4):661–663, 2002.

[30] G. Belomoin, J. Therrien, and M. Nayfeh. Oxide and hydrogen capped ultrasmall blue luminescent Si nanoparticles. *Applied Physics Letters*, 77:779, August 2000.

[31] İlker Doğan, Nicolaas J. Kramer, René H. J. Westermann, Kateřina Dohnalová, Arno H. M. Smets, Marcel A. Verheijen, Tom Gregorkiewicz, and Mauritius C. M. van de Sanden. Ultrahigh throughput plasma processing of free standing silicon nanocrystals with lognormal size distribution. *Journal of Applied Physics*, 113(13):134306, 2013.

[32] Jonathan G. C. Veinot. Synthesis, surface functionalization, and properties of freestanding silicon nanocrystals. *Chem. Commun.*, pages 4160–4168, 2006.

[33] Chung-Sung Yang, Richard A. Bley, Susan M. Kauzlarich, Howard W. H. Lee, and Gildardo R. Delgado. Synthesis of alkyl-terminated silicon nanoclusters by a solution route. *Journal of the American Chemical Society*, 121(22):5191–5195, 1999.

[34] V. Sivakov, G. Andrä, A. Gawlik, A. Berger, J. Plentz, F. Falk, and S. H. Christiansen. Silicon nanowire-based solar cells on glass: Synthesis, optical properties, and cell parameters. *Nano Letters*, 9(4):1549–1554, 2009. PMID: 19281253.

[35] Pavlo V. Antonov, Marc R. Zuiddam, and Joost W.M. Frenken. Fabrication of high-aspect ratio silicon nanopillars for tribological experiments. *Journal of Micro/Nanolithography, MEMS, and MOEMS*, 14(4):044506, 2015.

[36] B. J. Kim, J. Tersoff, S. Kodambaka, M. C. Reuter, E. A. Stach, and F. M. Ross. Kinetics of individual nucleation events observed in nanoscale vapor-liquid-solid growth. *Science*, 322(5904):1070–1073, 2008.

[37] E. Koren, G. Elias, A. Boag, E. R. Hemesath, L. J. Lauhon, and Y. Rosenwaks. Direct measurement of individual deep traps in single silicon nanowires. *Nano Letters*, 11(6):2499–2502, 2011. PMID: 21591656.

[38] Estelle Bourdon and Pierre Marie. Solution-Liquid-Solid Growth of Crystalline III-V Semiconductors: An Analogy to Vapor-Liquid-Solid Growth. 270(December):1619–1621, 2009.

[39] Allen J Bard, Larry R Faulkner, Elizabeth Swain, and Charity Robey. *Fundamentals and Applications*.

[40] Trasatti S. The absolute electrode potential: an explanatory note (recommendations 1986). *Pure and Applied Chemistry*, (58(7)):955–966, 2009.

[41] Cynthia G. Zoski. *Handbook of Electrochemistry*. Elsevier, Amsterdam, 2007.

[42] R.G. Compton and C.E. Banks. *Understanding Voltammetry*. Imperial College Press, 2011.

[43] M. Paunovic and M. Schlesinger. *Fundamentals of Electrochemical Deposition*. The ECS Series of Texts and Monographs. Wiley, 2006.

[44] David C. Grahame. The electrical double layer and the theory of electrocapillarity. *Chemical Reviews*, 41(3):441–501, 1947. PMID: 18895519.

[45] Thiruvengadam Munisamy and Allen J. Bard. Electrodeposition of si from organic solvents and studies related to initial stages of si growth. *Electrochimica Acta*, 55(11):3797 – 3803, 2010.

[46] J. Mallet, M. Molinari, F. Martineau, F. Delavoie, P. Fricoteaux, and M. Troyon. Growth of silicon nanowires of controlled diameters by electrodeposition in ionic liquid at room temperature. *Nano Letters*, 8(10):3468–3474, 2008.

[47] R.C. De Mattei, D. Elwell, and R.S. Feigelson. The synthesis of gaas by molten salt electrolysis. *Journal of Crystal Growth*, 43(5):643 – 644, 1978.

[48] Luyao Ma, Junsi Gu, Eli Fahrenkrug, and Stephen Maldonado. Electrochemical Liquid-Liquid-Solid Deposition of Crystalline Ge Nanowires as a Function of Ga Nanodroplet Size. *Journal of the Electrochemical Society*, 161(7):D3044–D3050, 2014.

[49] Eli Fahrenkrug, Janelle Biehl, and Stephen Maldonado. Electrochemical liquid–liquid–solid crystal growth of germanium microwires on hard and soft conductive substrates at low temperature in aqueous solution. *Chemistry of Materials*, 27(9):3389–3396, 2015.

[50] V. Schmidt, J. V. Wittemann, and U. Gösele. Growth, thermodynamics, and electrical properties of silicon nanowires. *Chemical Reviews*, 110(1):361–388, 2010. PMID: 20070117.

[51] Rw Olesinski, N Kanani, and Gj Abbaschian. The Ga-Si (Gallium-Silicon) system. *Journal of Phase Equilibria*, 6(4):362–364, 1985.

[52] J. P. Nicholson. Electrodeposition of silicon from nonaqueous solvents. *Journal of The Electrochemical Society*, 152(12):C795–C802, 2005.

[53] Mikhael Bechelany, Jamil Elias, Pierre Brodard, Johann Michler, and Laetitia Philippe. Electrodeposition of amorphous silicon in non-oxygenated organic solvent. *Thin Solid Films*, 520(6):1895 – 1901, 2012.

[54] Electrochemical reduction of silicon chloride in a non-aqueous solvent. *Electrochimica Acta*, 53(1):111 – 116, 2007.

[55] *The Merck Index*. The Royal Society of Chemistry, 2013.

[56] Mark W. Knight, Toon Coenen, Yang Yang, Benjamin J M Brenny, Maria Losurdo, April S. Brown, Henry O. Everitt, and Albert Polman. Gallium plasmonics: Deep subwavelength spectroscopic imaging of single and interacting gallium nanoparticles. *ACS Nano*, 9(2):2049–2060, 2015.

[57] Pae C. Wu, Christopher G. Khoury, Tong Ho Kim, Yang Yang, Maria Losurdo, Giuseppe V. Bianco, Tuan Vo-Dinh, April S. Brown, and Henry O. Everitt. Demonstration of surface-enhanced Raman scattering by tunable, plasmonic gallium nanoparticles. *Journal of the American Chemical Society*, 131(34):12032–12033, 2009.

[58] K F Macdonald, W S Brocklesby, V I Emel, V A Fedotov, and S Pochon. Gallium nanoparticles grow where light is. pages 1–11.

[59] Maksym Yarema, Michael Wörle, Marta D. Rossell, Rolf Erni, Riccarda Caputo, Loredana Protesescu, Kostiantyn V. Kravchyk, Dmitry N. Dirin, Karla Lienau, Fabian von Rohr, Andreas Schilling, Maarten Nachtegaal, and Maksym V. Kovalenko. Monodisperse colloidal gallium nanoparticles: Synthesis, low temperature crystallization, surface plasmon resonance and li-ion storage. *Journal of the American Chemical Society*, 136(35):12422–12430, 2014. PMID: 25133552.

[60] Paolo Ghigna, Giorgio Spinolo, Giovanni Battista Parravicini, Angiolino Stella, Andrea Migliori, and Richard Kofman. Metallic versus covalent bonding: Ga nanoparticles as a case study. *Journal of the American Chemical Society*, 129(25):8026–8033, 2007.

[61] A. Dargys and J. Kundrotas. *Handbook on Physical Properties of Ge, Si, GaAs and InP*. Science and Encyclopedia Publishers, 1994.

[62] A R Clarke. *Microscopy techniques for materials science*. 2002.

[63] J. Goldstein. *Scanning Electron Microscopy and X-ray Microanalysis: Third Edition*. Scanning Electron Microscopy and X-ray Microanalysis. Plenum, 2003.

[64] B.K. Agarwal. *X-ray spectroscopy: an introduction*. Springer series in optical sciences. Springer-Verlag, 1991.

[65] J.C. Vickerman. *Surface analysis: the principal techniques*. John Wiley, 1997.

[66] D. Briggs and M.P. Seah. *Practical Surface Analysis, Auger and X-ray Photoelectron Spectroscopy*. Practical Surface Analysis. Wiley, 1990.

[67] German Headquarters and Scienta Omicron Gmbh. XM1200 Monochromatic X-ray Source. 49(May), 2014.

[68] Scienta R Hipp and Hipp-Instrument Manual. SCIENTA HiPP-2 and HiPP-3.

[69] B. Predel. *Cu-Ga (Copper-Gallium)*, pages 1–8. Springer Berlin Heidelberg, Berlin, Heidelberg, 1994.

[70] Annett Thøgersen, Josefine H. Selj, and Erik S. Marstein. Oxidation effects on graded porous silicon anti-reflection coatings. pages 1–7, 2012.

[71] D. Briggs. Handbook of x-ray photoelectron spectroscopy c. d. wanger, w. m. riggs, l. e. davis, j. f. moulder and g. e.muilenberg perkin-elmer corp., physical electronics division, eden prairie, minnesota, usa, 1979. 190 pp. 195. *Surface and Interface Analysis*, 3(4), 1981.

[72] A. Namiki, K. Tanimoto, T. Nakamura, N. Ohtake, and T. Suzaki. XPS study on the early stages of oxidation of Si(100) by atomic oxygen. *Surface Science*, 222(2-3):530–554, 1989.

[73] Justin Henrie, Spencer Kellis, Stephen Schultz, and Aaron Hawkins. Electronic color charts for dielectric films on silicon. *Optics express*, 12(7):1464–1469, 2004.

[74] Linyou Cao, Pengyu Fan, Edward S. Barnard, Ana M. Brown, and Mark L. Brongersma. Tuning the color of silicon nanostructures. *Nano Letters*, 10(7):2649–2654, 2010.

[75] Tsvetanka Babeva, Hussein Awala, Marina Vasileva, and El Fallah. coatings and vapor responsive Bragg stacks. pages 8868–8876, 2014.